POST-OPERATIVE RENAL FUNCTION ANALYSIS USING VISIBLE DLP® HYPERSPECTRAL IMAGING SYSTEM

by

ABHAS THAPA

Presented to the Faculty of Graduate School of

The University of Texas at Arlington in Partial Fulfillment

of the Requirements for the Degree of

MASTER OF SCIENCE IN BIOMEDICAL ENGINEERING

THE UNIVERSITY OF TEXAS AT ARLINGTON

DECEMBER 2010

ACKNOWLEDGEMENTS

This research is a joint venture of UT Arlington and UT Southwestern. I would like to express my utmost gratitude to Dr. Karel J. Zuzak and Dr. Georgios Alexandrakis of UT Arlington along with and Dr. Jeffery Cadeddu of UT Southwestern for their support and guidance throughout the term of the research. I have learned from them not only the engineering and scientific aspect of data analysis but also the business aspect of work in terms of lab management and presentation of analyzed data.

I would also like to acknowledge the help I received from my colleagues; Robert P. Francis for guiding me in my initial venture through hyperspectral imaging, Eleanor Wehner for her help in editing, Vatsala Ranjanala for her help in re-analyzing a section of the data, Neil Jackson for his help in collecting clinical data, Naveen Balaji, Michael Mangum, and Kirstin Bradfield for their help and support. I would also like to extend my gratitude to Dr. Sara Best and Michael Holtzer for their help with collecting porcine open partial nephrectomy and laparoscopic data and Dr. Cadeddu and Dr. Ganesh Raj for their help in collecting valuable human open partial nephrectomy data. Moreover, I would like to express my sincere gratitude to Dr. Karel J. Zuzak and Dr. Edward Livingston for creating this research opportunity, which I believe will lead to a breakthrough technological advancement in the medical field.

Core funding for this project is provided by Texas Instruments (TI) and I would like to thank the people at TI: Arun Chhabra, Dylan Thomas and previous employees Shekar Rao and Jack Smith for their guidance and help in transitioning the instrument into industry. I would like to thank our collaborators at NIST: Dr. Maritoni Litorja and David W. Allen. We at the lab are also grateful to the companies Gooch and Housego (formally known as Optronics Laboratories), Photometrics, DVC Co. and AAVA technologies for the instruments used in this research and for software that collectively integrated these systems.

I would personally like to thank my father Achyut Thapa and my mother Ameeta Thapa for their immense support in pursuing a graduate degree in the United States of America. I cannot thank them enough for their support and their belief in me through every phase of my life.

November 14, 2010

ABSTRACT

POST-OPERATIVE RENAL FUNCTION ANALYSIS USING VISIBLE DLP® HYPERSPECTRAL IMAGING SYSTEM

Abhas Thapa, MS

The University of Texas at Arlington, 2010

Supervising Professor: Georgios Alexandrakis

Surgical and clinical settings in medical hospitals strive to keep up with technological innovations in order to improve the current healthcare scenario. Hyperspectral imaging (HSI) is a novel technology that addresses this problem. HSI is a non-invasive imaging technique that can provide information on both structural and functional conditions of tissue. This information is very useful particularly in live surgical procedures wherein the surgeons can get real-time feedback of the anatomical and functional changes of tissue, as they perform the operation. Currently available HSI systems are extremely slow and thus impractical for time restricted surgical or clinical uses. Hence, DLP® based HSI systems have been developed to make the imaging procedure much faster and more convenient. This work shows that the DLP® based HSI systems can operate at near video rate speeds making them practical for both clinical and surgical use.

The HSI system is based on the digital light processor (DLP®) technology developed by Texas Instruments. Two visible hyperspectral imaging systems have been described; one of the systems utilizes a CoolSNAP HQ2 camera; and this system has successfully been used in collecting data on open partial nephrectomies, in both humans and porcines.

Results from these experiments show that the visible HSI system can be used to predict post operative renal functions based on its ability to monitor changes in levels of tissue oxygenation. As a result of these positive findings on the utility of the HSI system, surgical interest has prompted the development of a laparoscopic DLP® HSI system. Preliminary data on porcine imaging, using the laparoscopic HSI system, demonstrate its ability to be used in live surgical settings; and other applications of both visible and near infrared (NIR) HSI systems prove the efficacy of this technology in multiple surgical and clinical settings.

TABLE OF CONTENTS

LIST OF ILLUSTRATIONS

Figure Page

LIST OF TABLES

CHAPTER 1

INTRODUCTION

A patient brought into a hospital in need of surgery is given a list of questions that need to be answered so that the doctor can make an educated decision based on the information provided. What if the patient was not aware of his/her pre-existing medical conditions? In the event of a surgical failure and even death, do we blame the surgeon for negligence? These questions may seem trivial to patients but it is critical to surgeons performing the surgery.

What if the surgeons could visualize in near real-time the conditions of tissue being operated? This would not just assist the surgeons to be aware of the pre-existing conditions of the tissue in question but surgeons could then change the course and method of the surgery in order to ensure better success. This particular research on the hyperspectral imaging system is an initiation to solving these very questions that will, in the future, assist surgeons during a live surgery. The data presented in this thesis was collected in live human open partial nephrectomies conducted at the UT Southwestern Zale hospital. Open partial nephrectomy data in porcine models are also presented, followed by preliminary data on laparoscopic surgeries on porcine models for transition into human laparoscopic surgeries.

A typical surgical procedure during an open partial nephrectomy is as follows:

A) The patient is brought into the room and the anesthesiologist sedates the patient in preparation for the surgery.

B) The surgeon performs incision on the abdomen on a specific side in order to access the kidney.

C) After the kidney has been located and is accessible, the hilum which consists of the renal artery and vein is clamped and the kidney is iced for approximately 8 to 10 minutes.

D) A surgical incision is performed on the area of the kidney based on a Computed Tomography (CT) image to excise the timorous tissue.

E) The excised tumor and the surrounding peritoneal fat on the kidney are sent to a pathology lab for analysis, to ensure that the entire tumor has been excised.

F) After suturing the incision on the kidney, using a surgical gauge, the clamp is removed from the hilum.

G) Finally, the abdomen is closed up.

Seems like a pretty standard procedure with a set protocol and steps. However, every surgical case is different and unique because a patient's medical history is unique. How then can the surgeons decide on the most effective procedure that needs to be adopted to ensure a successful surgery and a successful recovery?

Surgeons usually base their judgment on the medical history of the patient and the information that has been disclosed. The hyperspectral imaging system provides a new method of assisting the surgeons during a live surgery.

1.1 Hyperspectral Imaging

In order to understand hyperspectral imaging, it is undisputedly important to understand the concept of color. Students from the arts department might have a different interpretation of color, but students of science and engineering understand that color is the human brain's unique interpretation of different wavelengths of light. It is the biochemical reaction to these different wavelengths of light, in the cones of the retina of eye that creates a unique signaling in the visual cortex of the human brain, which then interprets and distinguishes color.

Just as the lens in the human eye focuses the light from an object to the retina, thereby creating an image for interpretation , the photo detector in modern cameras detect an object that is focused on it using an optical lens. The visual information from the cones in the eyes are interpreted as color by the brain. Analogous to the cones, the color information of the object in a camera is provided by various filters. With the advancement of these photo detectors, it is

possible to assign a unique spectrum to a unique color of an object. This spectrum is best understood in terms of either absorption or reflectance over various incremental wavelengths of light.

Hyperspectral imaging is hence the simultaneous imaging of different spectra in order to understand the change and/or characteristics of the target. Presently, hyperspectral imaging is used in many different disciplines such as physics, agriculture, mineralogy, and other military applications.

The hyperspectral imager presented in this thesis is a combination of an agile light source (OL490) and the detector (Camera system). The hyperspectral imager collects individual wavelengths as individual image frames, hence generating a 3 Dimensional data cube. A pictorial representation of the data is as shown in figure 1.1. The 3-Dimensional data cube is collected over a period of time and it consists of the overall spectral information of the target object.

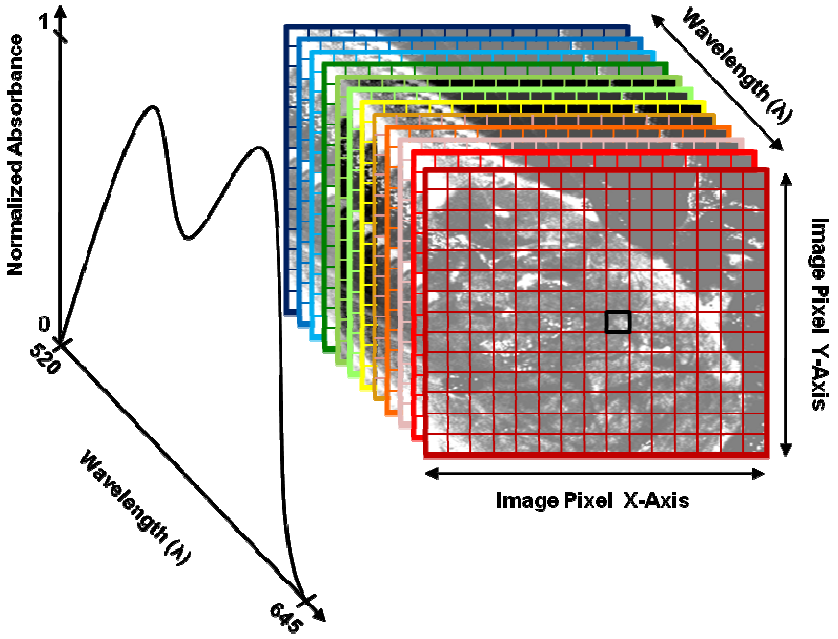

Figure 1.1 A three-dimensional hyperspectral cube (right) and the absorbance spectra (left) derived from this hyperspectral image cube
(Image of a well perfused human kidney)

1.2 Medical Application of Hyperspectral Imaging

A summary of a typical partial nephrectomy surgery mentioned previously explains only a fraction of the different clinical and surgical cases faced by hospitals. The ability of a surgeon to identify the different types of tissue structures during a surgery seems astonishing to most people; but it is understood that this ability is the result of years of academic and practical knowledge. Unlike a textbook image that clearly distinguishes and marks out different structures, a live surgery generally comprises of a lot of surrounding tissue and blood. The distinction between different tissues and organs is generally made by surgeons based on their visual cue and estimation. Hyperspectral imaging can be used to guide the surgeons by providing structural information based on the spectral information, the technology will better assist the surgeons in distinguishing the organs/tissue based on their biochemical composition. Furthermore, as described in the results in chapter 6, this technology can also help provide near video rate information on the biochemical changes in the tissue/organ overtime.

Although the data presented in this thesis is mainly focused on the biochemical (percent oxyhemoglobin) changes in the kidney, the technology is starting to gain popularity in other fields such as distinguishing different tissue structures during a cholecystectomy, determining the degree of tissue biochemical changes in burn victims, determining a better perfused skin flap to be used during plastic surgery. Along with the latter mentioned applications, the technology provides a possible use in Neurosurgery, Ophthalmology to detect diabetic retnopathy and Age-related Macular Degeneration (AMD) as well as many other new clinical and surgical fields of medicine.

1.3 Research Hypothesis

The Hyperspectral imager used for the collection of open partial nephrectomies is a visible system and the range of data collected using the system is 520 nm to 645 nm. This particular range of wavelength is chosen based on the previous Liquid Crystal Tunable Filter

(LCTF) system, and it contains distinctive absorbance peaks in the spectrum of both oxy and deoxyhemoglobin. The system is based on the Digital Light Processor (DLP®) technology by Texas Instruments and can be used to detect changes in percent oxyhemoglobin non-invasively. It takes 20 to 30 seconds to capture a 3-dimensional spectral cube and the system can capture up to 3 frames a second in the 3-shot mode. This real-time, non-invasive system can be used for real time imaging of biochemical changes in the tissue for clinical and surgical applications.

The research hypothesis is that the visible DLP® hyperspectral imaging system can be used for analyzing post-operative renal function based on its ability to provide real-time information on kidney oxygenation during partial nephrectomies.

CHAPTER 2

ILLUMINATION SOURCE

The OL490 is used as an illumination source for the system. The DLP® unit (OL490) was developed by Gooch & Housego (previously known as Optronics Laboratories, in Orlando, FL). The system consists of a lamp unit that uses a 500 Watt xenon lamp, along with a power supply for the lamp unit, and a DLP® unit that features the Texas Instruments (T.I.) DLP® Chip. The lamp unit is designed to couple with the DLP® unit and a desired slit can used to focus the broadband light from the Xenon lamp source onto the diffraction grating in the DLP® unit. Individual wavelengths of light from the diffraction grating is then projected on to individual columns of DMD micromirrors in the DLP® chip, which then allows the user to control the spectra of light spatially and/or temporally. The illumination source is hence used to illuminate the target with a precise spatial and temporal wavelength profile. Figure 2.1 explains the light path inside an OL490 Agile Light Source unit.

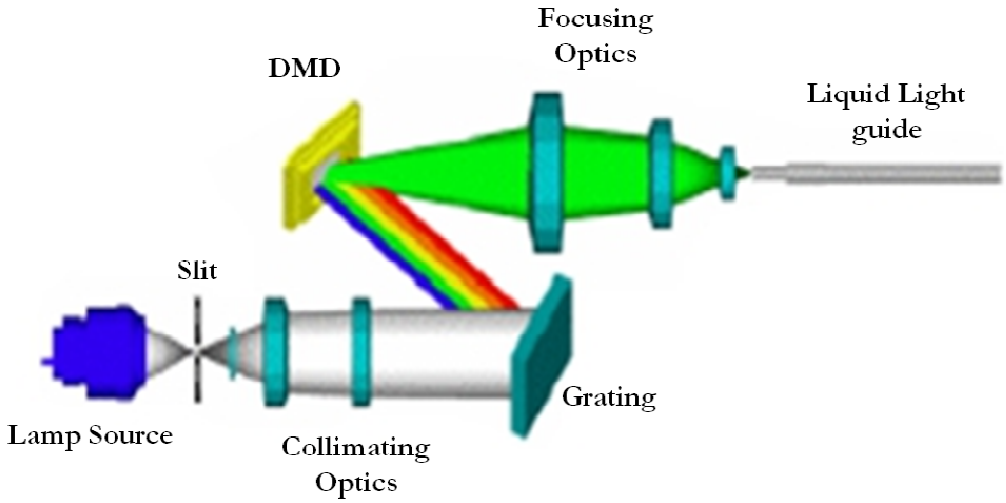

Figure 2.1 Light path of the OL 490 Agile Light Source from Xe lamp source to LLG output. [figure copied from [1]]

2.1 The Texas Instrument DLP® Technology

The DLP® Technology developed by Texas Instrument consists of the DLP® chip which is based on the Digital Micromirror Device (DMD) technology. The DMD was integrated into the DLP® chip (figure 2.2) by Larry Hornbeck of Texas Instruments, Inc. (Plano, TX) in 1987. The DMD consists of an m x n array of nearly 2 million microscopic mirrors that can be electronically switched on or off. This electronic control of the DMD mirrors allows the spatial and temporal modulation of light. As shown in figure 2.3, the micromirrors are made from aluminum and are hinge-mounted on to a CMOS substrate. Each individual mirror can be switched 'on' or 'off' very quickly by controlling the voltage bias, which creates an electrostatic attraction between the mirror and an address electrode and an opposite force between the yoke and an address electrode [3].

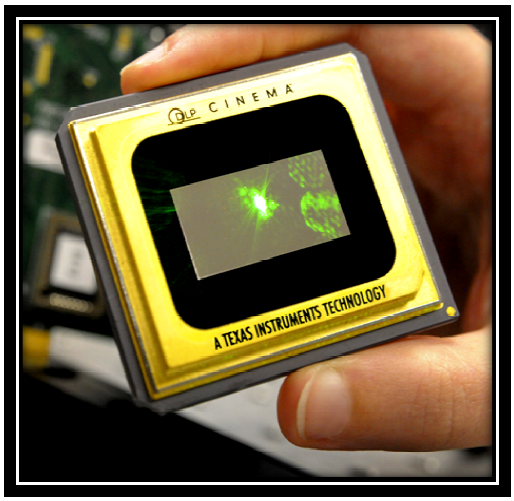

Figure 2.2 A digital light processor (DLP®) chip manufactured by Texas Instruments

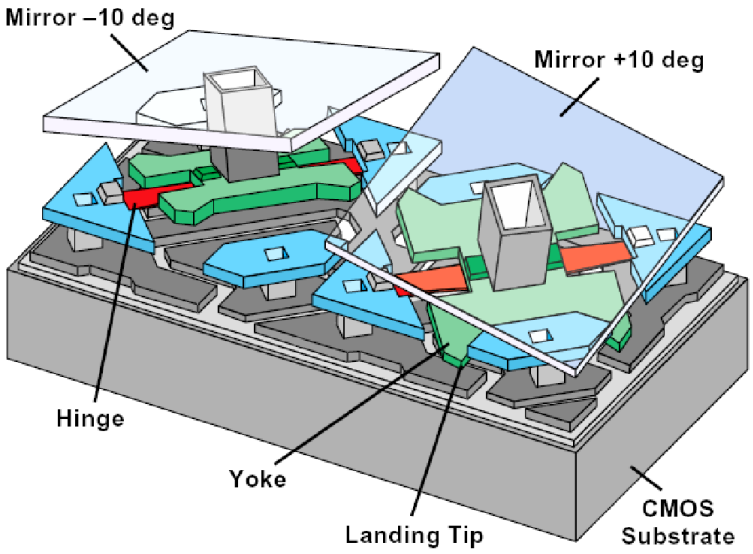

Figure 2.3 Two DMD pixels (mirrors are shown as transparent). [copied from [2]]. The mirrors are in different states shown at +/-10 deg, as in the original DMD design.
The mirrors in the DMD of the OL 490 hinge between +/-12 deg.

Specific directional deflection (positive and negative) of the micromirror is determined by the overall mechanical design of the DMD. Electrostatic force is developed between the mirror and its address electrode and also between the yoke and its address electrode. This produces a torque which acts against the restoring torque of the hinges hence allowing the mirror and the yoke to make positive and negative deflections. However, the mirror angle is constrained by the physical distance it is allowed to rotate. Both the mirror and the yoke rotate until the yoke rests on a mechanical stop, which is at the same potential as the yoke. Hence, the rotation angle of the mirrors can be determined very precisely. [2]

For purposes requiring spatial light modulation, light is focused on the DMD's array of mirrors, which are controlled to produce unique illuminations. This modulated light is then projected on to a target area via a projection lens. The angle and distance between the optics and DMD's array of mirrors are designed in such a way that when all of the mirrors are 'on' the entire target area is illuminated, and when all of the mirrors are 'off' none of the target area is illuminated. Desired sections of the target are illuminated, by turning 'on' the mirrors

corresponding to that section. Pulse width modulation is utilized for finer and more detailed modulation of light, which increases the grayscale levels for illumination (see Figure 2.4).

2.2 Spectral Selection Using the DLP® Unit (OL 490)

2.2.1 Hardware Specifications

The OL 490 consists of a DMD Discovery 3000 chip (Texas Instrument). This DMD Chip consists of a 768 x 1024 array of micromirros which can be rotated by +/- 12 degrees on its own 3.68µm pitch [2,4]. When a particular mirror on the DMD is turned 'on', the light that hits the mirror is reflected to the transmitting optics; and when a mirror on the DMD is turned 'off', the wavelength of light incident to that mirror is reflected to an internal heat sink. Hence, by assigning a particular wavelength of light to a column of micromirrors on the DMD chip, the intensity of that wavelength can be controlled by controlling the mirrors in that column. Hence the Chip acts as a spatial light modulator for spatial filtering.

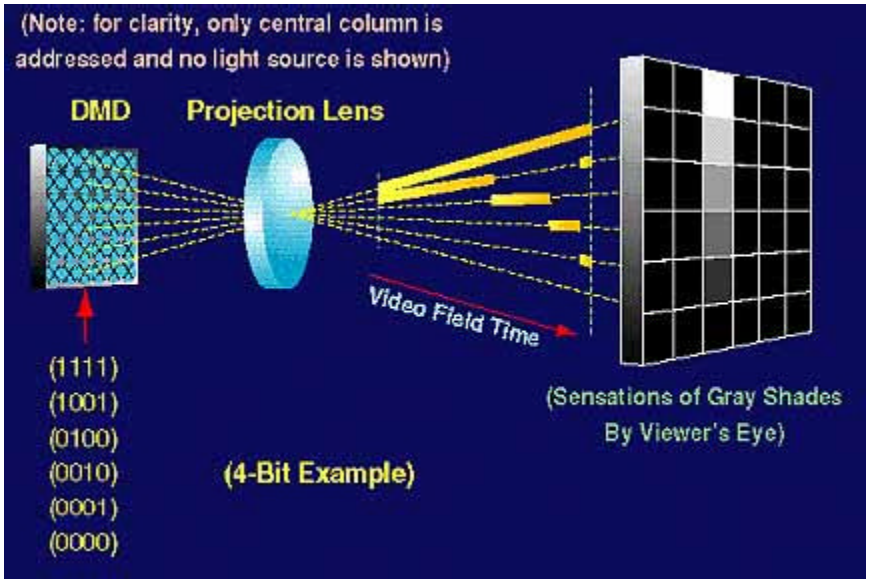

Figure 2.4 Example of DMD array projecting variable gray levels. [copied from [3]].

Spectroscopy deals with the effects of different wavelengths/frequencies of light on an object. Hence the first step of spectroscopy is the dispersion of light into several wavelengths. In

order to do this, broadband light passed through a thin diffraction grating or prism which is then angularly dispersed into different wavelength components. [5] In the OL490, the broadband light from the xenon source is projected onto a grating via a narrow slit. The slit size can be varied between 150µm, 350 µm, 500 µm, 750 µm. The larger the slit, the greater the light however, the bandwidth of individual bandpasses is also greater. The light projected onto the grating is then split into it individual wavelength/band components which is then projected onto the DMD chip. The intensity of the narrow bands or wavelengths of light is then controlled by the micromirrors on the DMD chip. For example: to illuminate with a particular wavelength of light at full intensity, all 768 mirrors of the column corresponding to that wavelength are turned on while all the other mirrors are turned off. This is a '1-bit' operation where micromirrors can either be 'on' or 'off' and the total number of intensity levels equals the number of micromirrors in a row, which in this case are 768.

Furthermore, In a 2-bit mode operation, the micromirrors in the DMD chip can be tilted at a different angle for 'half on' or 'half off' states allowing the user to have twice the number of intensity levels than in the 1-bit mode. Hence, in this case we can have 1536 levels of intensity. In the 2-bit mode of operation, although the intensity resolution is better, the micromirrors may require switching twice before the spectrum can be changed; so the time required for switching is doubled. The OL490 is capable of running at up to 6 bits, allowing modulations of 64 grayscale levels or 49,152 intensity levels. Since the time of illumination changed and since 768 levels were sufficient for data collection using our hyperspectral imaging system, the data that is being presented was collected with the OL490 running in1-bit mode. The Manufacturer specifications of the DLP® unit is as shown in table 2.1

Table 2.1 Optical output specifications from the manufacturer of the OL 490.

Spectral Range	380 nm to 780 nm
Spectral Accuracy	1 nm
Out of Band Rejection (@550 nm, output 450 nm)	~1000:1
Wavelength Resolution	0.39 nm
Intensity Control Levels	768 to 49 152 levels
Output Intensity (350 µm slit, all mirrors on)	~200 mW
Half-Bandwidths	
150 µm slit	~5 nm
350 µm slit	≤10 nm
500 µm slit	≤15 nm
750 µm slit	≤20 nm

2.2.2 Software Control of the DLP® Unit (OL 490)

An application software (AS) and a software development kit (SDK) are provided with the DLP® unit. The SDK consists of applications written in C# programming language and the dynamic link libraries (DLLs) necessary to control the OL 490 hardware. The AS is a graphical user interface (GUI) that allows the user to control the spectral illumination from the DLP® unit either spectrally or temporally. The DLP® unit is connected to a computer via a USB 2.0 link. Before the operation of the unit, the user must load in the appropriate calibration profile for the slit being used by clicking on cogwheel icon on the application and selecting the appropriate slit size from a drop down menu. The calibration profile in the application determines the wavelength corresponding to the micromirror column in the DMD chip for the selected slit size.

The user can control the spectral illumination of the light from the DLP® unit by adjusting the render slider or by inputting the values of wavelength ranges, intensity levels and bandwidth. A tab-delimited text file, that specifies these values, can also used to control the unit. For the visible system, the slider can be used to select wavelengths ranging from 380nm to 780nm, bandwidth values ranging from 5nm to 200nm, and intensity values ranging from 0 to 100. If the user can create a specific spectral profile using multiple bands, by setting these three parameters and saving it to a list displayed on the right hand side of the AS. Using the render slider is useful to create simple spectral illuminations (one or two bands). To create a more complex illumination

spectrum, the user can create a tab-delimited text file that specifies the wavelengths and their corresponding intensity levels.

The tab-delimited text file is called a Gwectra file and has an extension of “*.gxt”. The Gwectra file consists of a two columns of values. The first column of values consists of the 1024 wavelengths corresponding to 1024 columns of the DMD chip. The second column consists of fixed point values of up to 2 decimal places ranging from 0.00 to 100.00 which correspond to the percentage of mirrors that are turned on for the specific wavelengths on the first column. The five preceding header lines in the Gwectra file specify the compatible software version and when the file was created. The onscreen snap shot of the AS GUI is shown in Figure 2.5

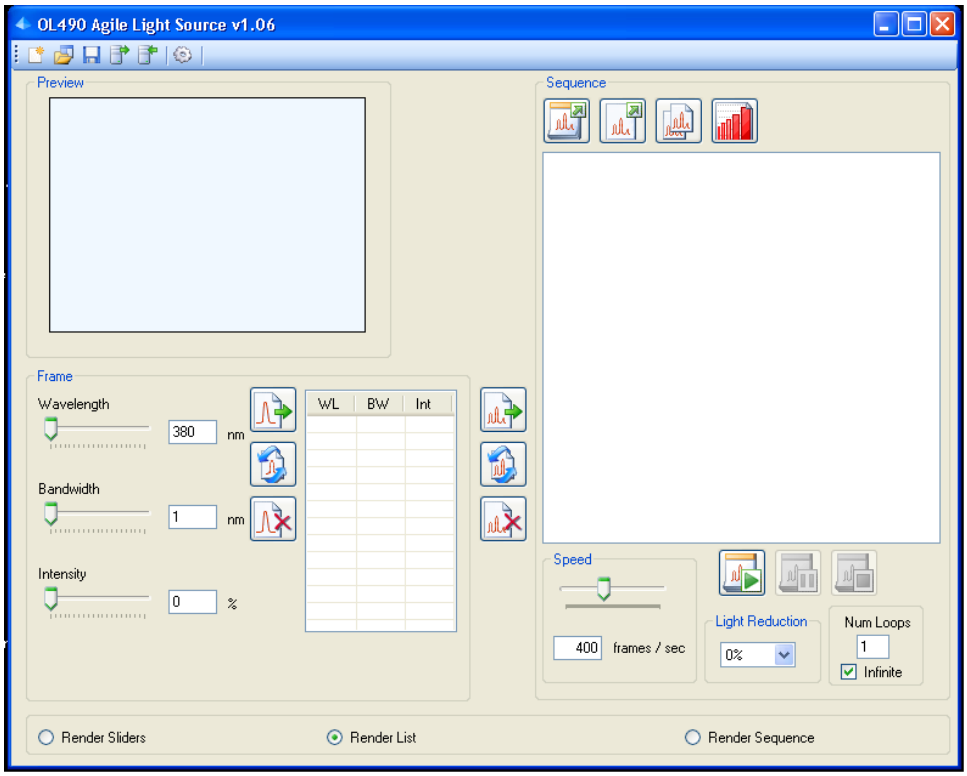

Figure 2.5 Screen shot of OL 490 AS GUI.

The desired spectral illumination can be achieved by loading in the frames or Gwectra files on the right of the AS window. The controls on the bottom right of the window allows the user to control the speed of spectral changes from 1 frame per second to 12, 500 frames per second,

the percentage of light reduction and the number of loops for the entire sequence. The percentage of light reduction reduces the light intensity for all wavelengths equally. Linear light reduction can be adjusted in the settings window can be used to flatten the spectral illumination profile.

The user can also use the “Create Sweeps” button, on the top far right corner of the AS window, to sweep through contiguous bandpasses with constant intensity and bandwidth. The user can define the sweep by specifying the start and end center wavelength, the wavelength increment and the intensity value for each bandpass.

2.2.3 Characterization of the DLP® Unit (OL 490)

A brief overview of the system characterization results have been presented in this thesis. For a detailed characterization please refer to the thesis “DLP® Hyperspectral Imaging for Surgical and Clinical Utility” by Robert P. Francis.[6]

Since the OL 490 is coupled with a lamp unit that features a xenon lamp which has a spectral dependence on temperature and time, a photodiode test was conducted for the stability of the OL490 for different temperatures over time. The photodiode tests are performed using a 350 µm slit. The OL490 is programmed to output a bandpass centered at 580nm with a bandwidth of 10nm and 33% intensity. This illumination bandpass is selected based on the photodiodes improved response at that particular wavelength and the expected use of the system from 520 nm to 645 nm to collect spectral differences between oxy- and deoxyhemoglobin. The intensity is chosen to be 33% so that the maximum amplified photodiode voltage response is close to 9 Volts so that it does not overload the amplifier.

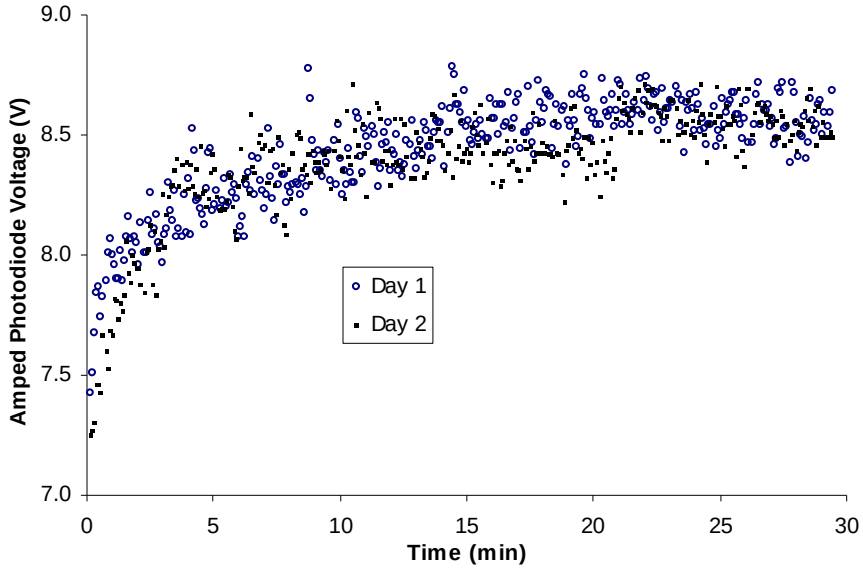

Figure 2.6 Amped photodiode voltage measured “From Cold” as OL 490 lamp source is switched on and left illuminating 580 nm, 10 nm bandwidth, at 33% for 30 minutes.

The results shown in figure 2.6 are from the “From Cold” experiments conducted over two days with the lamp in the system running from the cold state (beginning of the experiment for each day) and figure 2.7 shows the results for the “From Warm” experiments for the consecutive runs after the first experiment in each day.

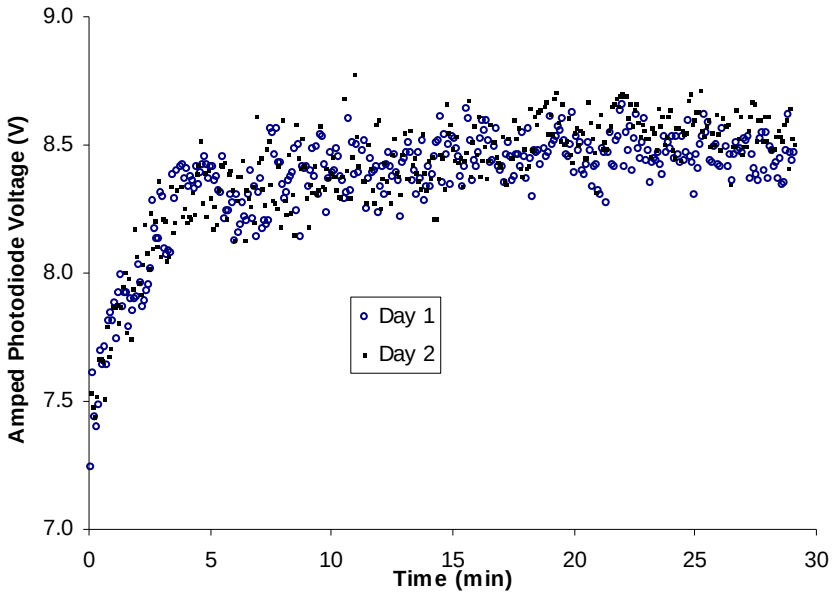

Figure 2.7 Amped photodiode voltage measured "From Warm" (average of 3 runs) as OL 490 lamp source is switched on and left illuminating 580 nm, 10 nm bandwidth, at 33% for 30 minutes.

The plots indicate that there is only a small variance in the data from both days and that the OL490 requires about 15 minutes reaching steady state "From Cold" and about 5 to 10 minutes to reach steady state "From Warm". [6]

To find the difference in the output intensity when using each of the four available slits (150 µm, 350 µm, 500 µm, and 750 µm), all the 1024 wavelengths are turned to 80% intensity and the visible spectrometer reading are recorded. The output spectral illuminations for the different slits are as shown in figure 2.8.

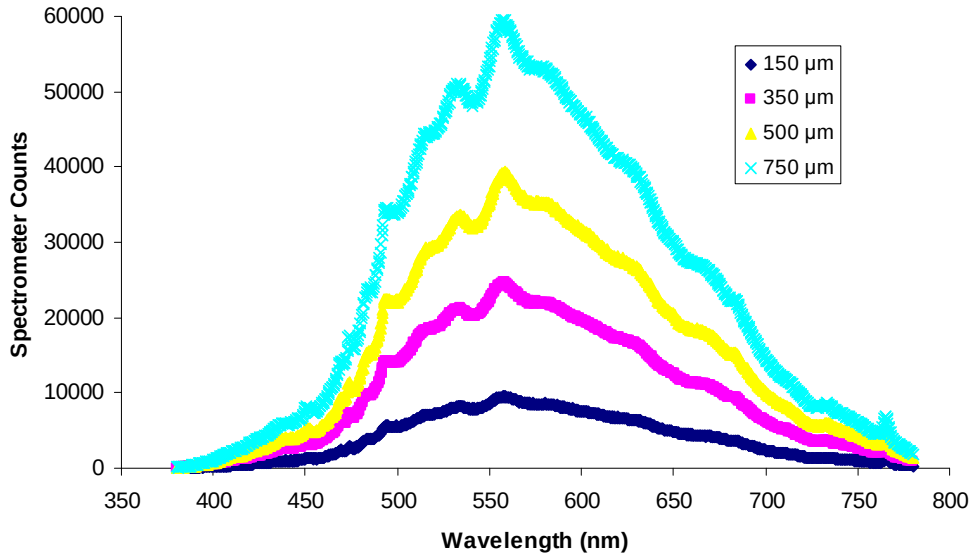

Figure 2.8 Spectrometer responses of illumination spectrum output with all mirrors on for each slit.

From Table 2.2 we can see that the 350 µm slit allows 2.5 times more light through the optics head than the 150 µm slit, the 500 µm slit allows 3.99 times more light through, and the 750 µm slit allows 5.95 times more light through.

Table 2.2 Ratio of spectrometer response to OL 490 illumination spectrum 'AllOn.gxt' between each slit and the narrowest slit (150 µm).

	Slit Width			
	150 µm	***350 µm***	***500 µm***	***750 µm***
Mean	1.00	2.50	3.99	5.95
St. Dev.	0.00	1.61	2.32	2.55

The minimum bandwidth test for each slit is also performed to check the systems performance over manufacturer's specifications. For this test, the full-width half maximum (FWHM) bandwidth for each measured bandpass spectrum is calculated as

$$FWHM = \left|\lambda_2 - \lambda_1\right|$$

where λ_1 and λ_2 are the wavelengths that correspond to half of the maximum intensity measured by the spectrometer. The 2500+ Visible spectrometer response is too low to get an accurate

measure of FWHM for wavelengths below 420 nm and above 720nm; so only values for 420 nm to 760 nm are considered for this experiment. Figure 2.11 shows that the measured minimum bandwidth is relatively constant over different wavelengths for a given slit and lower than the manufacturer's specifications.

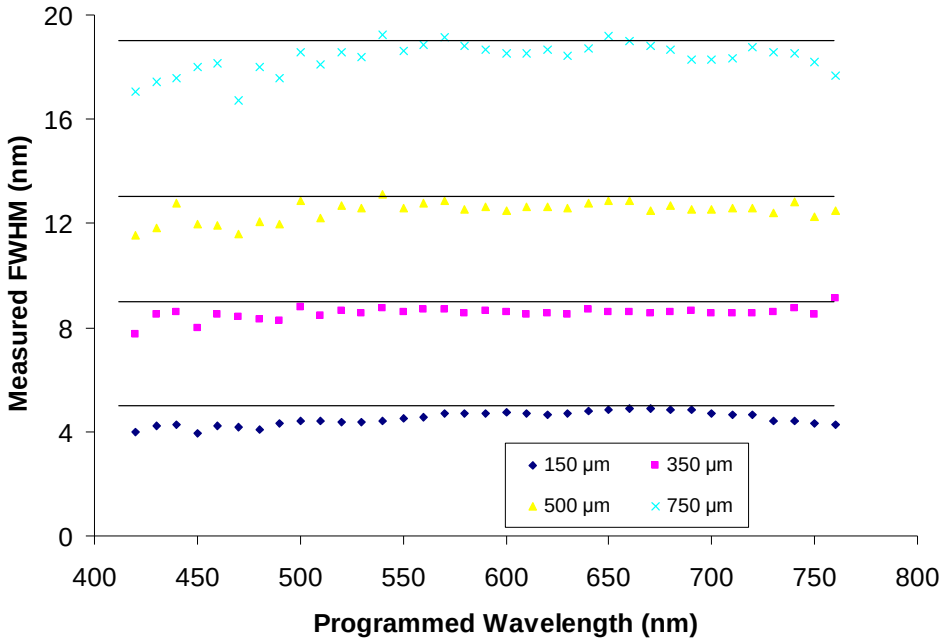

Figure 2.9 Measured FWHM bandwidths for OL 490 AS programmed center wavelength bandpasses from 420 nm to 760 nm in 10 nm increments.The programmed bandwidths (5 nm, 9 nm, 13 nm and 19 nm) are shown as horizontal line segments.

For practical use, the minimum bandwidth on the OL 490 should be set to a higher value than the minimum programmable bandwidth specified by the manufacturer. [6]

It is hence observed that, although the amount of light increases with the increase in slit size, it also increases the bandwidth of the wavelengths diminishing the spectral resolution of the system. Since the DLP® based visible hyperspectral imaging system was based on the already existing LCTF based visible hyperspectral imaging system which has been optimized over a period of ten years[9,12,13]; and operated at 10nm increments, the 350 µm slit was selected in order to collect the open partial data presented in this thesis.

CHAPTER 3

DETECTORS

The visible DLP® based data hyperspectral system used for imaging, primarily featured a CoolSNAP HQ_2 camera. The system based on this CoolSNAP HQ_2 camera was used for collecting the human and porcine open partial nephrectomies data that is being presented in chapter 6. Based on this system, a smaller and lighter version of the visible DLP® based data hyperspectral system using a DVC camera was also developed. The DVC system has also been featured in this thesis and its primarily been developed for laparoscopic imaging applications, and has been used in porcine laparoscopic surgeries. The DVC Camera consists of the same Sony ICX285 CCD Chip as the HQ2 camera but consists of a very small form factor and requires minimal to no cooling.

3.1 The CoolSNAP HQ_2 Camera

The CoolSNAP HQ_2 camera is considered for the visible DLP® system after considering its benefit over the PIXIS 1024BR camera, which was being used as part of the LCTF based visible hyperspectral imaging system. The characterizations of both the PIXIS 1024 BR and the CoolSnap HQ2 have been presented in detail in the thesis "DLP® Hyperspectral Imaging for Surgical and Clinical Utility" by Robert P. Francis.[6] The characterization of the DVC laparoscopic system and the HQ2 visible system are presented in this thesis.

Table 3.1 Comparison of imaging specifications of detectors for integration into DLP® HSI.

Model	PIXIS 1024BR	CoolSNAP HQ2
CCD Sensor	Back illuminated; deep depletion	Sony ICX285
Pixel Array	1024 x 1024	1392 x 1040
Pixel Size	20 x 20 µm	6.45 x 6.45 µm
Imaging Area	20.5 x 20.5 mm	8.98 x 6.71 mm
A/D Transfer	16 bits @ 2 MHz	14 bits @ 20 MHz

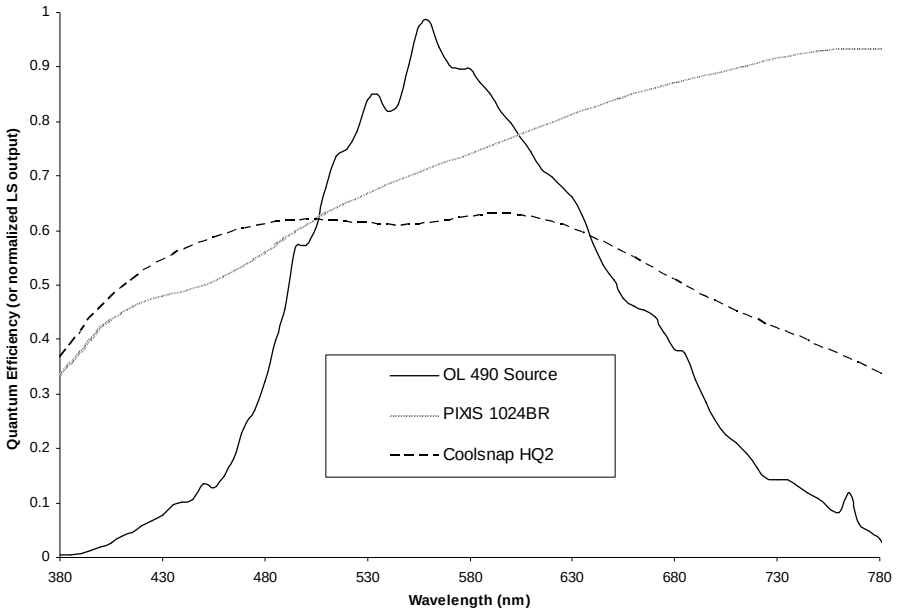

Figure 3.1 Quantum efficiency curves of the OL490, PIXIS 1024BR and Coolsnap HQ2

3.2 The DVC Camera

The DVC 1500M camera is used for the laparoscopic visible system after the successful use of the HQ2 camera in porcine and human open partial nephrectomies. The DVC camera has a smaller form factor in comparison to the HQ2 camera, making it very useful as a hand held device for the laparoscopic applications of hyperspectral imaging. The DVC 1500M is a monochrome camera that features the same Sony ICX285 CCD chip as the HQ2. However, the system has a 12 bit digitizer compared to the 14 bit digitizer in the HQ2.

Table 3.2 Comparison of imaging specifications of detectors for integration into DLP® HIS System.

Model	DVC 1500M	CoolSNAP HQ2
CCD Sensor	Sony ICX285	Sony ICX285
Pixel Array	1392 x 1040	1392 x 1040
Pixel Size	6.45 x 6.45 µm	6.45 x 6.45 µm
Imaging Area	8.98 x 6.71 mm	8.98 x 6.71 mm
A/D Transfer	12 bits @ 40 MHz	14 bits @ 20 MHz

In order for the hyperspectral system to be useful to the surgeons, the speed of the system is critical. To capture a single hyperspectral image cube, multiple wavelength images are captured over time, so the speed of the system detector is dependent on the time required to capture individual images. According to the manufacturer specifications,

$$r = \frac{n}{t_{readout}} \qquad \text{equation 3.1}$$

According to the specifications for the HQ2, r = 35 fps for a full-frame image binned 4 x 4. In order to determine the dependence of frame rate on exposure time, the time to collect 100 full FPA frames with 4 x 4 binning was measured at various exposure times. As with previous experiments on the HQ2 Camera, a stop watch with 1/100th sec resolution was initiated with the left hand while acquisition was started by clicking the laptop mouse button with the right hand. The stop watch was stopped with the left hand when the laptop display visually signaled acquisition was complete. Four runs at each exposure time (1 ms to 13 ms in 1 ms increments) were timed, the frame rate for each run was calculated by equation 3.1 and the mean for each exposure time was plotted as shown in Figure 3.2. From the figure, it is evident that the DVC frame rate is not dependent on detector exposure time, but the HQ2 frame rate decreases as exposure time increases. This is probably because the DVC camera is much faster compared to the HQ2 camera.

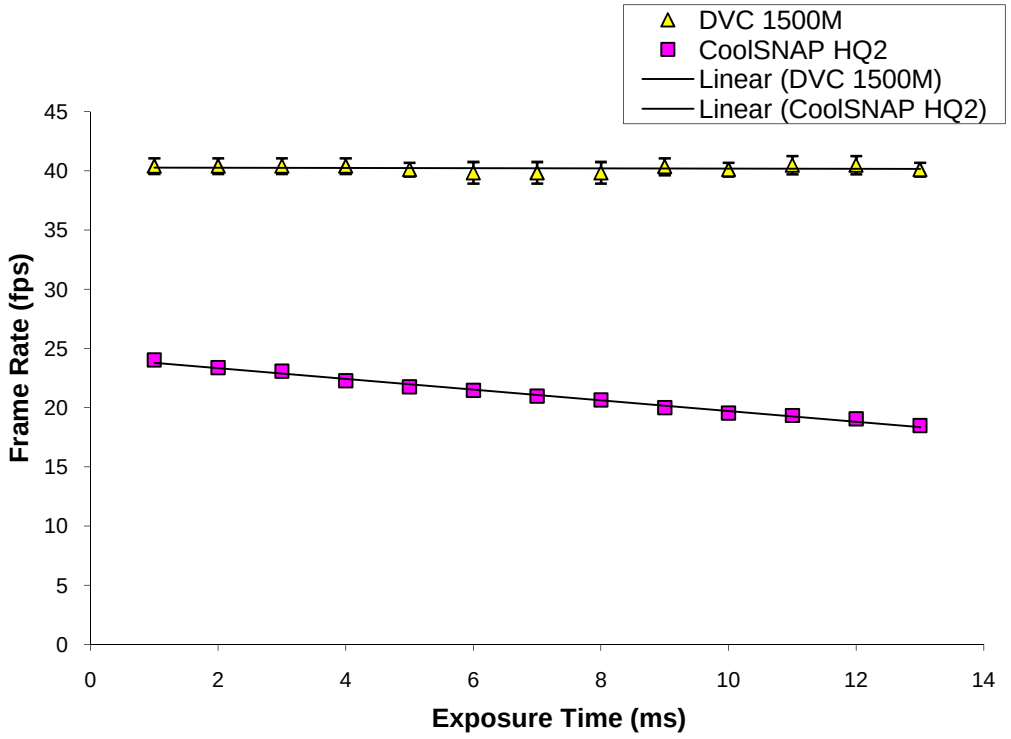

Figure 3.2 The dependence of camera frame rate on exposure time for the CoolSnap HQ2 and DVC 1500M (time to acquire 100 frames measured using a stop watch).

In another experiment, the exposure time was set to a constant 8 ms and the number of frames acquired (*n*) was varied to determine the static and dynamic constants associated with each camera. The static constant (*S*) refers to the time required to initialize capture and display on monitor that acquisition is complete. Readout time ($t_{readout}$) depends on the value of *S* only once, no matter the value of *n*. The dynamic constant (*D*) refers to the time required to open shutter, expose the CCD array, close shutter, and convert the analog signal array to a digital image. Since all of these actions occur once for every frame, $t_{readout}$ depends on the value of *D* times the value of *n*. The relationship should be linear according to equation 3.2.

$$t_{readout} = D \cdot n + S \qquad \text{equation 3.2}$$

The results from this second set of stop watch tests are shown in Figure 3.3. From the highly correlated linear fit of each camera's data set, we show that the relationship is indeed

linear. Assuming that the static constant is mostly a function of human response time with the stop watch, and the current software being used to acquire, S_{DVC} and S_{HQ2} are not indicative of the respective camera's maximum frame rate.

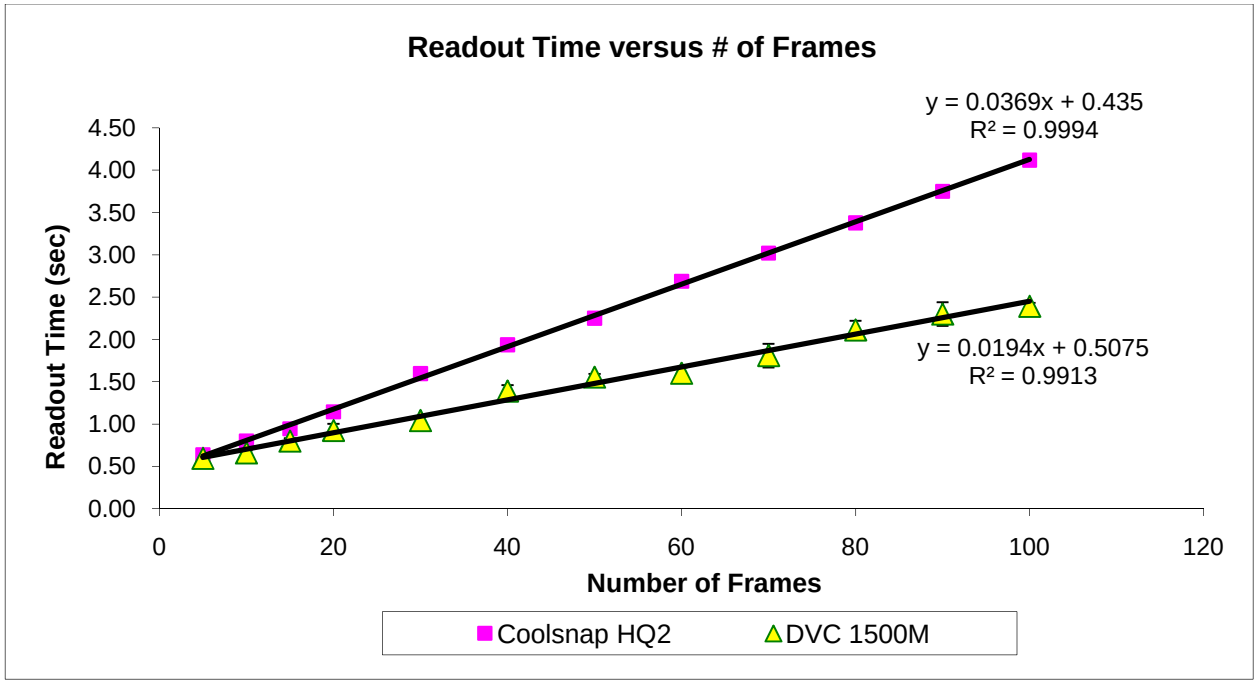

Figure 3.3 Results of second set of stop watch speed tests, Where exposure time remained constant and number of frames varied. The slope of each linear fit is used to calculate ideal frame rate of the cameras.

Empirical results from this second stop watch speed tests also indicate that the DVC is much faster than the HQ2 as the number of frames increase.

CHAPTER 4

HYPERSPECTRAL IMAGER

(AN INTEGRATION OF THE ILLUMINATION SOURCE AND DETECTOR)

4.1 System Description

The DLP® hyperspectral imaging system (DLP® HSI) used for collecting data on open partial nephrectomies has been explained in detail in the thesis by Francis, RP.[6] The system consists of a spectral illuminator providing spectroscopic light to the sample and a focal plane array detector capturing reflected spatial image information that are synchronized by a computer program. The image detector is a CoolSNAP HQ2 (Princeton Instruments, Trenton, NJ) with a Sony ICX285 CCD sensor, 1392 x 1040 array with 6.45 µm x 6.45 µm pixels, with a dual-speed 14 bit or 12 bit, 20 MHz or 10 MHz digitizer. The spectral illuminator is an OL-490 Agile Light Source (Optronic Laboratories, Orlando, FL) with a spectral range of 380 nm to 780 nm with a full width half maximum bandpass of 10 nm when using a 350 µm slit. Computer software was developed by AAVA Technology (Plano, TX) specifically for managing the spectral illumination, data collection and image processing. Figure 4.1 shows the mechanically integrated system, in which the CoolSNAP image detector along with a standard 50 mm lens (Nikon, Melville, NY) and liquid light guide (LLG) beam shaping illumination optic are mounted side-by-side on a friction head atop a mobile Samson tripod (Quickset International, Northbrook, IL). The DLP® Agile light source along with battery backup systems and power supplies are placed on a standard Rubbermaid® cart (Winchester, VA) providing the system the ability to be easily transported within and between surgical and clinical suites.

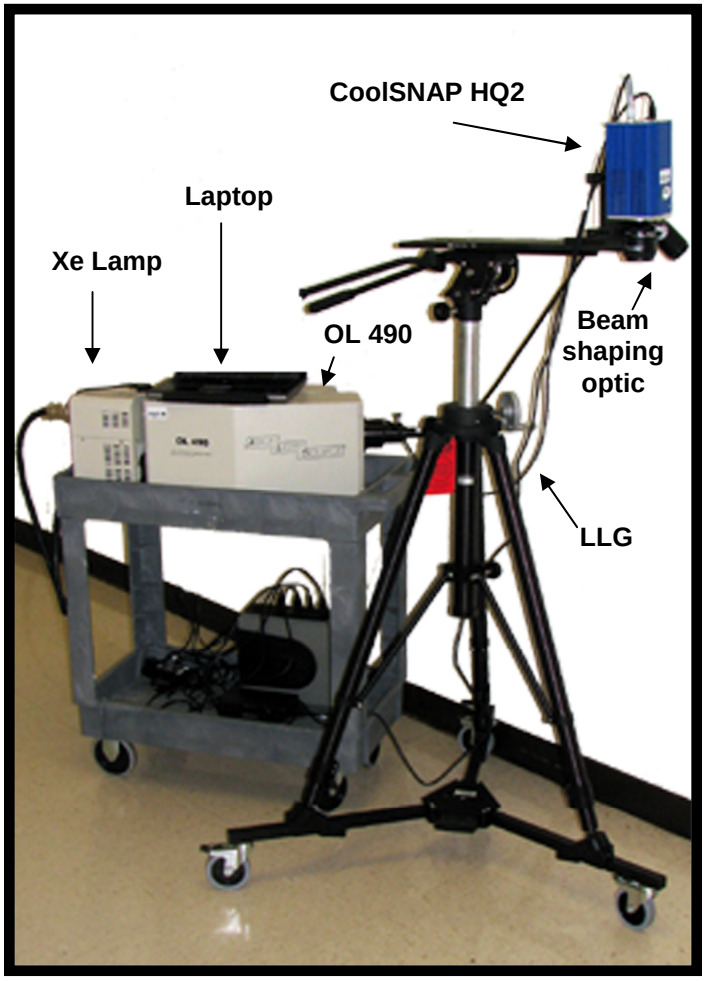

Figure 4.1 Mechanically integrated DLP® hyperspectral imaging system (DLP® HSI).

Based on this system, a smaller system was designed for laparoscopic applications. The image detector in the laparoscopic system consists of a DVC Camera (DVC Co.) that consists of the same Sony ICX285 CCD sensor, 1392 x 1040 array with 6.45 μm x 6.45 μm pixels, with a 12 bit, 20 MHz or 40 MHz digitizer. The spectral illuminator is an OL-490 Agile Light Source (Optronic Laboratories, Orlando, FL) with a spectral range of 380 nm to 780 nm with a full width half maximum bandpass of 10 nm when using a 350 μm slit. Computer software was developed by AAVA Technology (Plano, TX) specifically for managing the spectral illumination, data collection and image processing. The main difference between the systems is that the system used for open partials is software triggered while the laparoscopic system is hardware triggered.

Figure 4.2 shows the mechanically integrated system, in which the DVC camera is coupled with a 0 degree Karl Storz 10mm laparoscopic probe and a Karl Storz light guide. The DLP® Agile light source along with battery backup systems and power supplies are placed on a standard Rubbermaid® cart as in the system used for open partials. Having the small form factor allows the DVC system to be a hand held device during surgical applications.

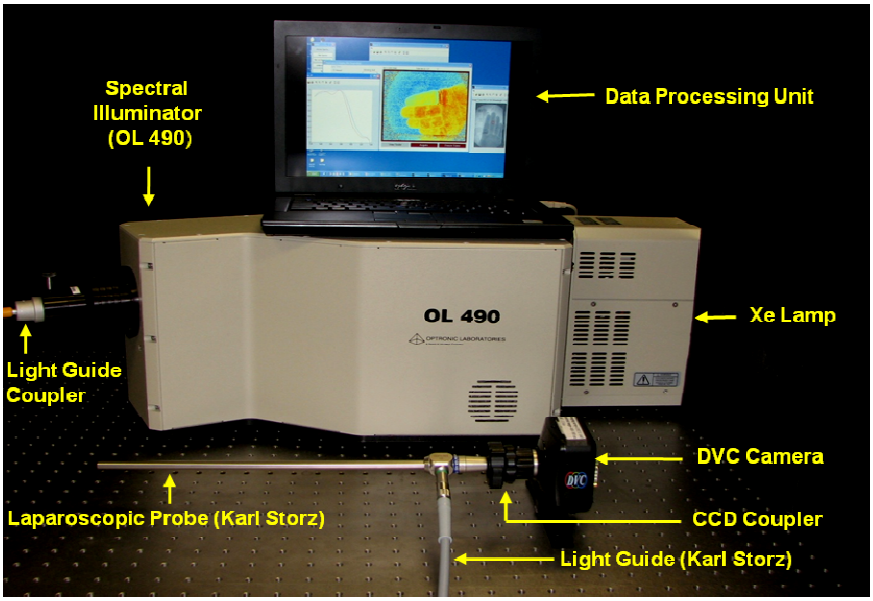

(a)

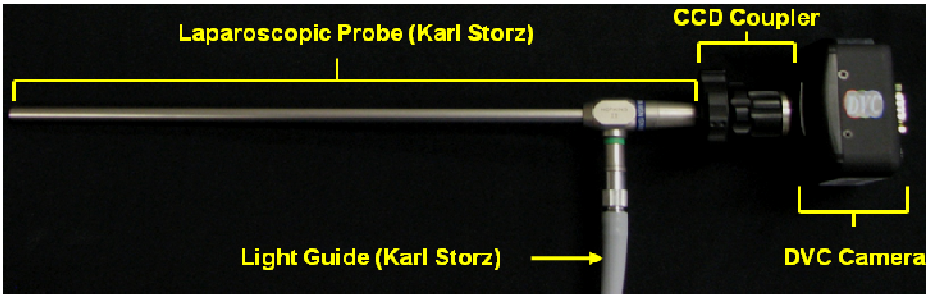

(b)

Figure 4.2 The DVC hyperspectral imaging system used for laparoscopic imaging (a). A closer view of the camera, coupler, laparoscopic probe and fiber optic light guide (b).

4.2 Hardware and Software Synchronization

A graphical user interface (GUI) was written for Windows XP in C# programming language by AAVA Technology (Plano, TX). This GUI synchronizes the illumination and image capture, saves the hyperspectral image cube, and processes with new and existing MATLAB algorithms. The GUI allows the user to control the DLP® unit as well as the camera simultaneously by setting necessary illumination schemes, and camera acquisition parameters. The GUI contains a window where a Windows bitmap image is displayed in one of two modes: "View Finder" or "Acquire". In "View Finder" mode, the displayed image is the most recent raw grayscale image acquired by the camera in free running mode with the light source illuminating broadband white light. The GUI allows the user to select a pre-written processing algorithm to run (see Figure 4.3) and so based on this processing algorithm, in the "Acquire" mode, the displayed image is the result of a processed hyperspectral image cube with the light source illuminating according to a certain sequence of spectral illuminations.

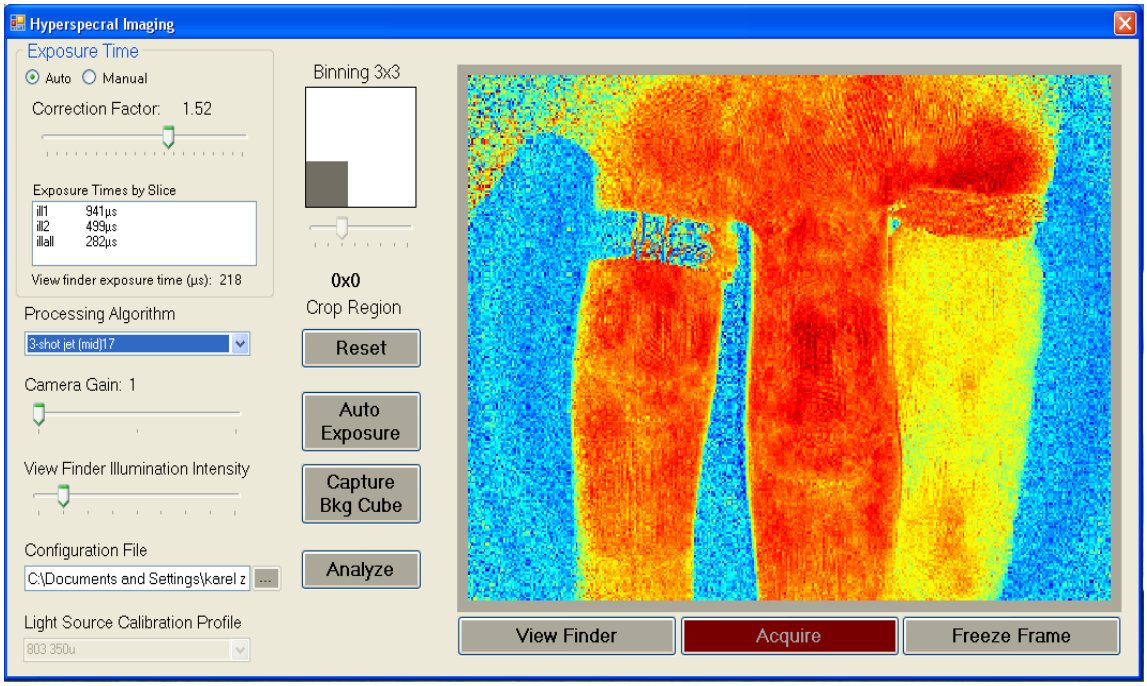

Figure 4.3 Screen shot of GUI for DLP® hyperspectral imaging system.

OL 490 illumination schemes are programmed in the form of a configuration file (*.ini) which contains the following lines of text:

```
[Analyzer Parameters]
x=348
y=260
exptype=1
numframes=126
startwave=520.0
endwave=645.0
incwave=1.0
software version=1
bandwidth=10.0
SpectrumDefType=Parametric
```

Here, ‘X’ and ‘Y’ initialize the horizontal and vertical pixel dimensions of the output image, ‘numframes’ describes the number of illumination spectra (and images) in a single sequence, and ‘SpectrumDefType’ can have a value of ‘Parametric,’ indicating a sweep of contiguous bandpasses, or ‘Arbitrary,’ indicating a sequence of complex broadband spectral illuminations. If the value is ‘Parametric,’ then ‘startwave,’ ‘endwave,’ and ‘incwave’ indicate the wavelength range and increment of a sweep in nm, while ‘bandwidth’ describes the bandwidth of each bandpass. If the value for ‘SpectrumDefType’ is ‘Arbitrary,’ the other values have little meaning and an additional list of the *.gxt filenames must be appended to the lines of text in the configuration file.

Camera gain, binning and exposure time are controlled by their respective sliders in the Hyperspectral Imaging GUI. Exposure time has the most complex control because it can be variable by slice of the hyperspectral cube, or constant in all images. If the radio button ‘Auto’ is selected in the ‘Exposure Time’ control box, the exposure time for each slice of the hyperspectral

cube is defined by the list of illuminations and corresponding times in µs. This list can be augmented manually by opening up the currently loaded *.ini file in a text editor or automatically by clicking the 'Auto Exposure' button in the middle of the GUI. Clicking the 'Auto Exposure' button causes the system to acquire a hyperspectral image cube with the currently loaded illumination scheme and a constant 20 µs exposure time. The average intensity of each image in the cube is calculated, and a new list of variable exposure times is generated to correct for any variation in intensity values. Specifically, lower intensity image slices get increased exposure times, while saturated image slices get decreased exposure times. The theory behind the 'Auto Exposure' algorithm is valid, but it incorrectly assumes that exposure time can be incremented in 1 µs steps. Due to the stair step phenomenon shown in section, clicking 'Auto Exposure' often results in incorrect values for exposure time. If the radio button 'Manual' is selected in the 'Exposure Time' control box, the exposure time for each slice is constant.

Finally, the processing algorithm is selected from a pull down menu that is populated with a list of programmed MATLAB routines. New and augmented algorithms can be added to the list by creating a new 'hsi.dll' file in MATLAB and loading it into the Windows system path. Key processing algorithms are 'Show 1st Raw Image', which simply reads the hyperspectral cube and displays the first slice with maximum contrast; 'Show Absorbance', which reads the hyperspectral cube and a previously acquired reference cube, calculates absorbance for each slice, and displays the average absorbance across the spectral dimension; 'Oxyz Jet', which processes a cube of contiguous bandpass images and results in an image color-coded for tissue oxygenation; and, '3shot Jet - *', which processes a cube of three complex spectral illumination images and results in an image color-coded for tissue oxygenation.

4.3 Color Tile Test

The DLP® Hyperspectral system was used to capture spectra of known standards (color tiles) from the National Institute of Standards and Technology (NIST). The characterization and calibration of the Visible HQ2 system for Imaging open partial nephrectomies has been explained in the thesis by Francis, RP.[6] The system was calibrated by capturing hyperspectral images of

four standard NIST color tiles with known reflectance spectra shown in figure 4.4. The DLP® Hyperspectral Imager was programmed to perform a "Full Spectral Sweep," in which the OL-490 performed an illumination sweep through a series of fifty-one (n = 51) center wavelengths over the full spectral range of the system, 450 nm to 650 nm, at 10 nm bandpass and incrementing by 4 nm. A background image cube of a 99.9% reflectance Spectralon target (Labsphere, Inc., North Sutton, NH) is acquired as the sample path. Five consecutive image cubes of the color tiles are acquired and used to calculate the reflectance spectra of each tile. The reflectance spectra measured by the system are compared to their corresponding standard spectra by calculating the root mean square error (RMSE)[23] between the two spectra:

$$RMSE = \sqrt{\frac{\sum_{n=1}^{51}(R_{DLP,n} - R_{NIST,n})^2}{51}} \qquad \text{equation 4.1}$$

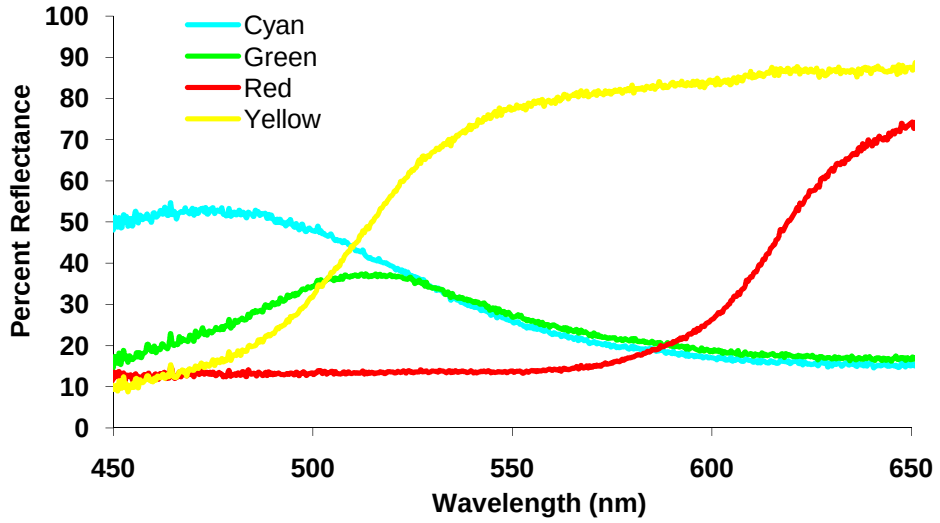

Figure 4.4. Reflectance spectra of four standard color tiles in the operating range of the DLP® HSI as measured by NIST.

The Spectral measurements of these tiles using the DLP® Hyperspectral Imaging system consisting of the HQ2 Camera is as shown in figure 4.5

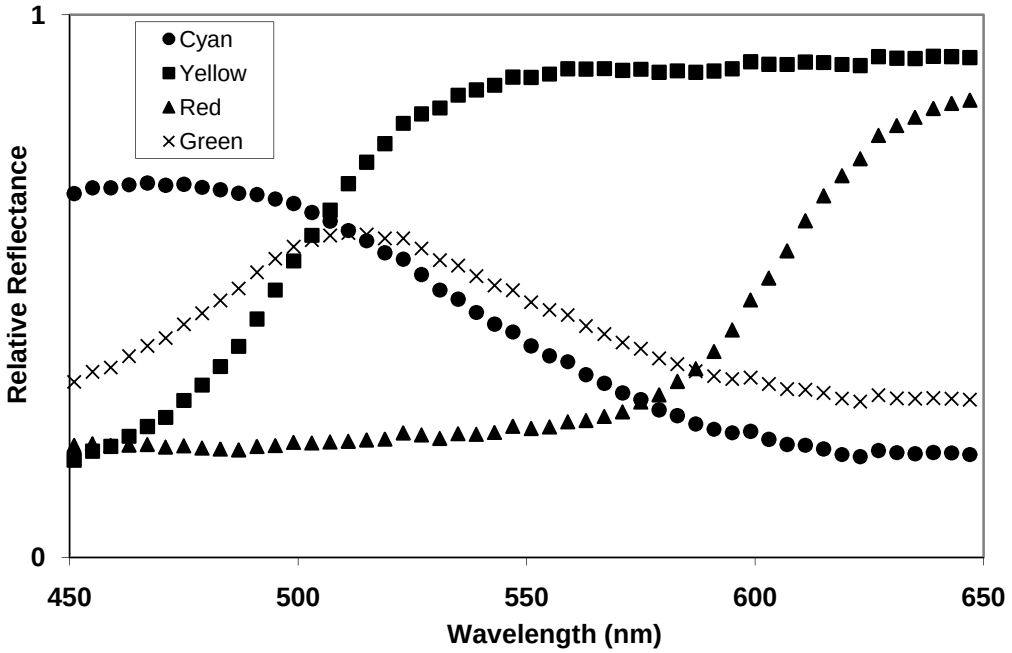

Figure 4.5 Reflectance spectra of four standard color tiles in the operating range of the DLP® HSI as measured by DLP® Hyperspectral Imager for Open Partial Nephrectomy.

The Working of the GUI on the Laparoscopic system is very similar to the system used for the open partials. However, in the latter system, the DLP® unit (OL490) is hardware triggered from digital pulse from the DVC camera. This new feature allows the system to be operated much faster than the previous system, consisting of the HQ2 system. Furthermore, the auto exposure mode in the GUI cannot be used for the DVC Laparoscopic system, due to the cameras inability to set different exposure times for individual frames of a cube. Other issues with the DVC cameras have been quantified and the company DVC co has been notified of these issues that affect the overall speed of the system in specific applications.

With the Illumination source (OL490) remaining constant, a color tile reflectance test is performed on the laparoscopic system as well. The plot for this test is as displayed in figure 4.6

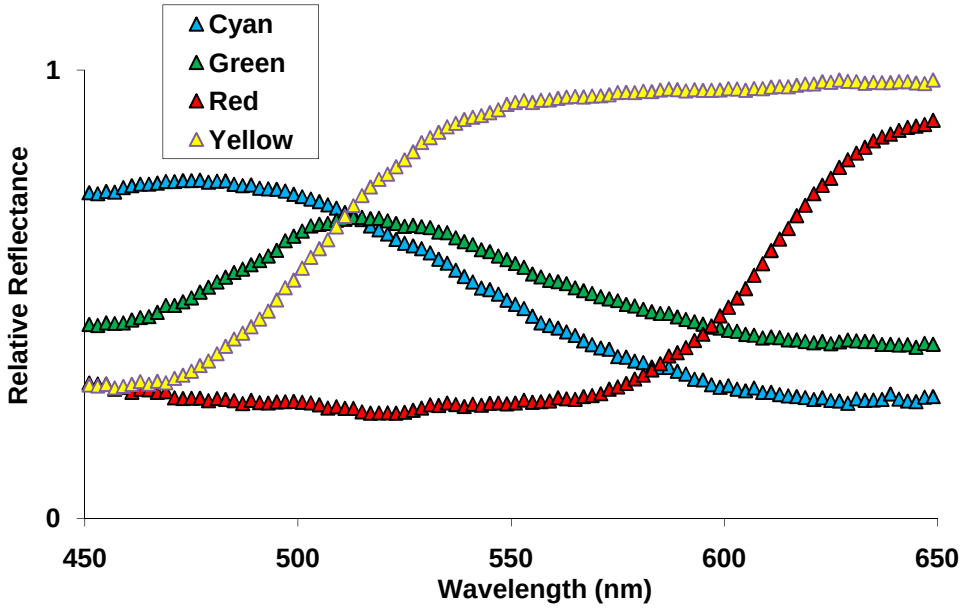

Figure 4.6 Reflectance spectra of four standard color tiles in the operating range of the DLP® HSI as measured by the DLP® Hyperspectral Imager for Laparoscopic Nephrectomy.

From figures 4.5 and 4.6 it is clear that both the systems are very similar. Hence, the system calibration on the DVC laparoscopic system should follow the previous HQ2 system used for collecting data on the open partials.[6]

4.4 Spatial Resolution of DVC Camera System

A standard method to determine spatial resolution of an imaging system is to use a line pair gauge to create a modulation transfer function of the percent contrast visualized by the system versus frequency of line pairs.[17] A Karl Storz Endoscope was attached to the c-mount of the DVC Camera via a standard laparoscopic coupler. These set of optics focused the image field of view (FOV) onto the focal plane array (FPA) of the camera. Grayscale images of a white background (Figure 4.a) and the line pair target (Figure 4.b) were captured at focal distances of 6cm. Using the same method described in previous theses,[6,18,19] a USAF 1951 target (Edmund Optics, Barrington, NJ) was imaged to determine minimum spatial resolution of the DVC 1500M integrated with the visible OL 490. The target was illuminated with broadband light from

380 nm to 780 nm from the OL 490, and the DVC camera was programmed with an exposure times and gains as mentioned in Table 4.1.

Table 4.1 Experimental parameters of the DVC laparoscopic HSI system for computing percent contrast

	Binning			
Parameters	**1x1**	**2x2**	**3x3**	**4x4**
Acquisition Exposure Time	22ms	22ms	13ms	7ms
Gain	15.5dB	3dB	0dB	0dB

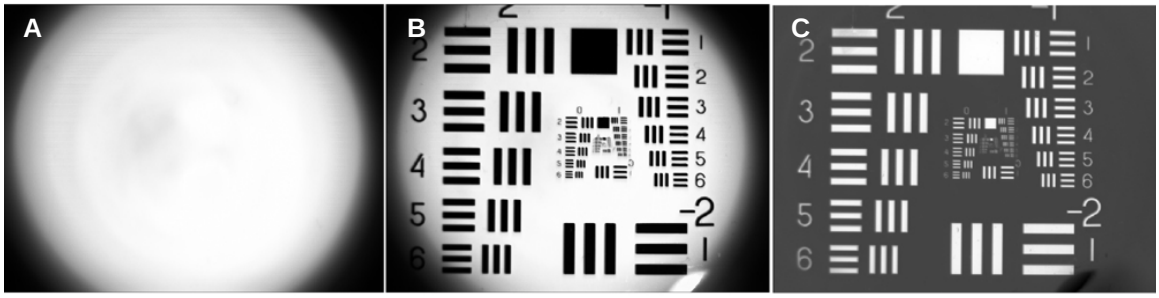

Figure 4.7 Grayscale images of (a) white background and (b) USAF 1951 target are ratioed to create an (c) absorbance image. Images are captured at a 6 cm focal distance.

In MATLAB, the absorbance image (figure 4.7 c) was analyzed to determine the percent contrast between the vertical white bars and the dark background for each line pair. The percent contrast value for each line pair was calculated according to equation 4.2, where I_{max} is the maximum pixel intensity from a white bar in the image and I_{min} is the minimum pixel intensity from the dark space in between the white bars.

$$\%C = \frac{I_{\max} - I_{\min}}{I_{\max} + I_{\min}} \times 100\% \qquad \text{equation 4.2}$$

Each line pair width is precisely defined on the quartz line pair target, so the result of equation 4.2 for each line pair was plotted as function of spatial resolution as shown in figure 4.8. As expected, the percent contrast drops off sharply as the line pair width decreases. Polynomial fits of the data for each binning parameter was calculated to extrapolate the minimum spatial resolution, defined as the size of an object which can be identified with at least 20% contrast.

The minimum spatial resolution was found to be approximately 0.2 mm for 6 cm focus with 4x4 binning, 0.17 mm for 6 cm focus with 3x3 binning, 0.15 mm for 6 cm focus with 2x2 binning and 0.11 mm for 6 cm focus with 1x1 binning. This indicates that the minimum spatial resolution is directly proportional to the binning. Due to restrictions in MATLAB memory, which ran out if individual images were captured with no binning, we used 4x4 binning as a standard while collecting data for the laparoscopic system.

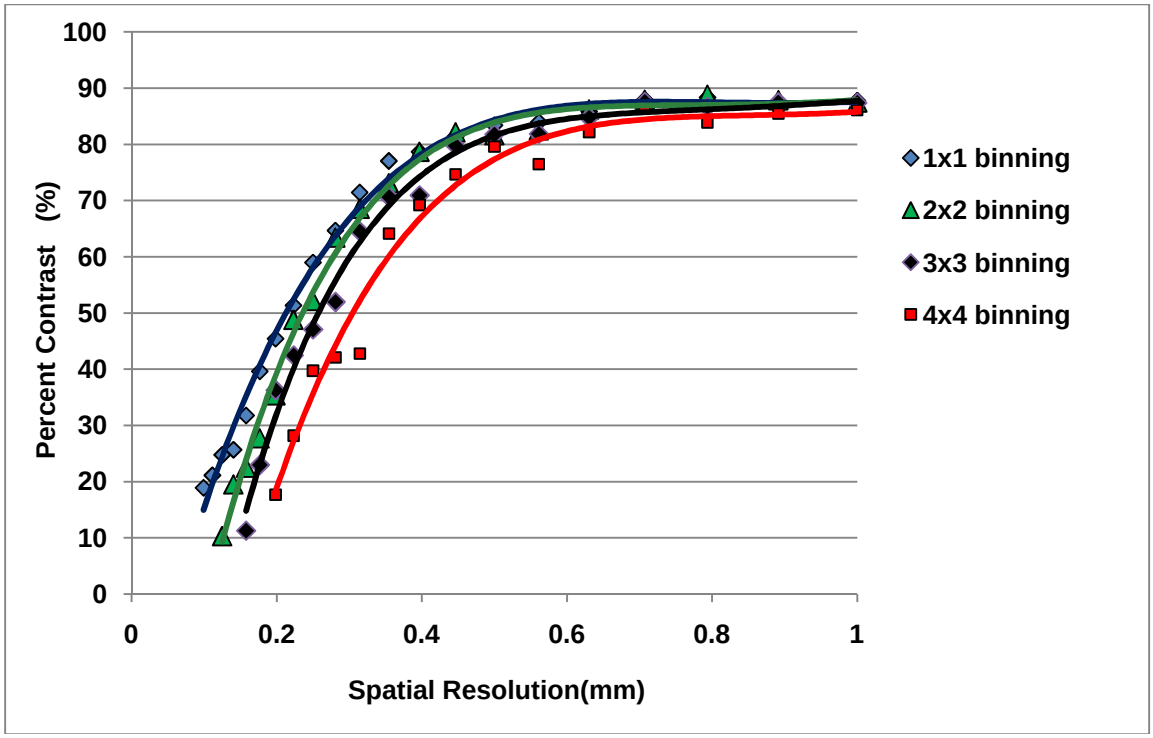

Figure 4.8 Spatial resolution of the DVC camera, determined by percent contrast at different levels of binning.

CHAPTER 5

DATA ACQUISITION AND PROCESSING

5.1 Data Acquisition

5.1.1 Imaging procedure

Based on the characterizations on the OL 490, regardless of which illumination method is used, the following imaging procedure is standard for both systems. Prior to imaging, the OL 490 lamp must be turned on for a period of 10 minutes and at least 20 minutes for the first imaging session of the day, see section.[6] In order for the synchronization software to recognize the drivers for the camera and light source, both the camera and the OL 490 optics head must be switched on at least 20 seconds prior to starting the software in Windows. The software takes a while to initialize the first time it is loaded. On startup, the GUI is always in 'View Finder' mode with camera parameters set in a saved startup file. The GUI will not open if it encounters errors associated with hardware and software DLLs or unrecognizable parameters in the startup file.

After all hardware components are running and the GUI window is visible on the screen, the first step is to focus the camera by adjusting the lens; so that objects at the operating distance of the system are clear. It is important that this operating distance remains constant throughout the entire imaging session. If the image on the screen is dark or saturated, the exposure value of the detector can be augmented by adjusting the lens aperture, the camera binning or gain, and the 'View Finder Exposure Time' under the 'Manual' exposure setting. It is generally preferred to keep binning at 4 x 4 in order to prevent an overload on the memory of the processor.

The next step is to load the configuration file based on the desired illumination method. While loading the configuration file, a 99.9% reflectance target (spectralon) is placed in the field of view of the camera. The beam shaping optic that focuses the output illumination from the LLG is adjusted so that the beam spot on the reflectance target is in the center of the detector array for

the system used in open partial nephrectomies. This is not an issue in the laparoscopic system, as it involves illumination via the Karl Storz endoscope. 'Capture Bkg Cube' is clicked and the OL 490 begins to sequence through programmed illumination spectra at the same time the camera begins to acquire one image per illumination spectrum. When the background cube has been completely captured, 'Processing Algorithm' is set to 'Show 1st Raw Image' and 'Acquire' is clicked to begin acquisition with the 99.9% reflectance target remaining in the FOV. After completion of one acquired cube, stand alone processing is initialized with the 'Analyze' button to check for saturation in each slice of the cube. If the maximum count measured is greater than or equal to 14,300 for the HQ2 system or 4000 for the DVC system, the exposure value must be decreased to avoid saturation, but if the maximum count measured is lower than 12,000 for the HQ2 system or 3500 for the DVC system, the exposure value should be increased to take advantage of the full well capacity of the detector. In 'Manual' exposure, the exposure time is adjusted by explicitly changing the exposure time of the detector. . In the HQ2 system, for the 'Auto' exposure mode, the exposure time is adjusted by increasing or decreasing the correction factor so that all of the variable exposure times maintain correct proportion to each other. However, this feature is not applicable to the DVC system due to the camera's inability to change exposure times between individual frames within a cube, without significantly delaying the overall acquisition time. The process of acquisition and analysis of the spectralon target is repeated until the ideal exposure time and lens aperture is determined. Finally, 'Capture Bkg Cube' is clicked again to overwrite the initial background cube with a background cube acquired using the ideal parameters.

Once the correct background cube has been captured, the spectralon target is removed from the FOV and the system is redirected upon a sample area of interest (i.e. tissue). The appropriate processing algorithm, based on the illumination scheme is selected and the acquisition is initialized. 'Processing Algorithm' may be changed at any moment during acquisition, as long as the new algorithm is appropriate for the illumination method in the current configuration file. For example, the 'Oxyz Jet' is only appropriate for an illumination method

containing 126 contiguous bandpasses and if this processing algorithm is used with the 3 shot method, it will cause a processing error and an exception violation is visible on the screen. If the processing algorithm is changed during acquisition, the first output bitmap is a grayscale image representing the raw image acquired when the first illumination spectrum of the sequence is output from the OL 490. Processed bitmap images are continuously displayed in the visualization area of the GUI until 'Freeze Frame' is clicked. 'Freeze Frame' freezes the current visualization bitmap and allows the user to probe the image by pressing 'Analyze' or switch to a new configuration file, saving the last five sample cubes acquired. Every bitmap that is displayed is also saved in the "output" folder in the same parent directory as the configuration file.

5.1.2 Illumination methods

Three illumination methods have been implemented in the Visible DLP® Hyperspectral Imaging system: Full Spectral Sweep, Spectral Sweep, and 3 Shot. New illumination methods based on different requirements can easily be created by programming the spectral light engine. This ability of the system to change the illumination spectrum to any imaginable narrow or broadband spectrum in the wavelength range of the OL 490 makes it faster and more flexible to different applications. This versatility has allowed the DLP® HSI to be used for a number of imaging applications.

5.1.2.1 Full Spectral Sweep

The full sweep for the visible OL490 spans its rated wavelength range of 380 nm to 780 nm. Since we utilize a 350µm slit, the Full Spectral Sweep method sweeps bandpass illuminations with 10 nm bandwidth. The wavelength increments can be as small as 1nm. Hyperspectral image cubes acquired with this method explicitly measure the absorbance spectroscopy of an area of interest. After dividing it with the background, each slice in the cube represents the absorbance of the bandpass illumination at which the image is acquired. Thereby, each spatial pixel in the processed cube represents a discrete absorbance spectrum of the tissue or other material in the physical position corresponding to that pixel. Since the output intensity of the OL 490 is wavelength dependent with very low intensities near the extremes of its wavelength

range (see figure 2.8), the ends of each absorbance spectrum are considered less reliable than the data near the middle of the wavelength range.

This illumination method can be used to help calibrate the system as a spectrophotometer. An algorithm to process its image cubes for visualization of oxygen content can be developed; but this method takes very long; so the 126 method is used instead. However, with the spectral information acquired using Full Spectral Sweep illumination, it is possible to search for new spectral signatures of chemical chromophores and develop new processing algorithms.

5.1.2.2 Spectral Sweep

Since the DLP® visible hyperspectral systems are developed based on the LCTF-based hyperspectral imaging systems, the Spectral Sweep method sweeps bandpass illuminations with 10 nm bandwidth from 520 nm to 645 nm in 1 nm increments. A hyperspectral image cube acquired with this method consists of 126 slices and is hence also referred to as the 126-shot method. This 126-shot method measures the absorbance spectroscopy of an area of interest. After dividing the background, each slice in the cube represents the absorbance of the bandpass illumination at which the image is acquired. Each spatial pixel in the processed cube represents a discrete absorbance spectrum of the tissue or other material in the physical position corresponding to that pixel. Each pixel absorbance spectrum is then compared to a known reference spectra for oxy- (HbO_2) and deoxyhemoglobin (Hb) by multivariate least squares analysis to calculate the percent HbO_2 for that pixel. The processing algorithm used with this method is the ‘oxyz’ algorithm.

5.1.2.3 3 Shot

Surgical venues generally require data to be collected as fast as possible in order to avoid the surgery duration which in turn translates into costs. Since both the full sweep and the 126 shot method take time to capture, a 3 Shot method is developed which utilizes the functionality of the DLP® unit (OL490) to be programmed to illuminate with a complex broadband spectra in the wavelength range from 527nm to 638nm. The 3 Shot method of illumination basically corresponds to the illumination with two positive differences between the known

absorbance spectra for oxy and deoxyhemoglobin and an illumination with all wavelengths at 50% intensity. A hyperspectral image cube acquired using this method consists of 3 frames and these frames can be used to calculate the percent of HbO_2 for each spatial pixel without having to measure the absorbance spectra. The following illuminations are programmed into the OL490 by loading a configuration file with 'SpectrumDefType=Arbitrary':

$$L_{1,3shot} = \sum_{n=8}^{119} L_{OL490}(\lambda_n) V_1(\lambda_n) \quad (5)$$

$$L_{2,3shot} = \sum_{n=8}^{119} L_{OL490}(\lambda_n) V_2(\lambda_n) \quad (6)$$

$$L_{3,3shot} = \sum_{n=8}^{119} L_{OL490}(\lambda_n) \quad (7)$$

As shown in figures 5.1, $V_1(\lambda_n)$ represents absolute difference spectra resulting from subtracting the normalized absorbance spectra of deoxyhemoglogin from that of oxyhemoglobin and $V_2(\lambda_n)$ represents the absolute difference spectra resulting from subtracting the normalized absorbance spectra of oxyhemoglogin from deoxyhemoglogin. The limits of summation are set from 8 to 119 since the reference spectra has been filtered using a moving average filter that trims seven discrete values from both the beginning and end of the total range of the spectra.

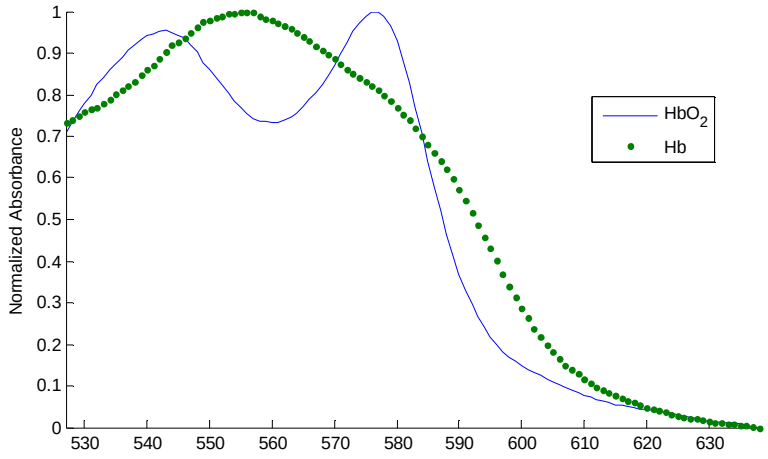

(a)

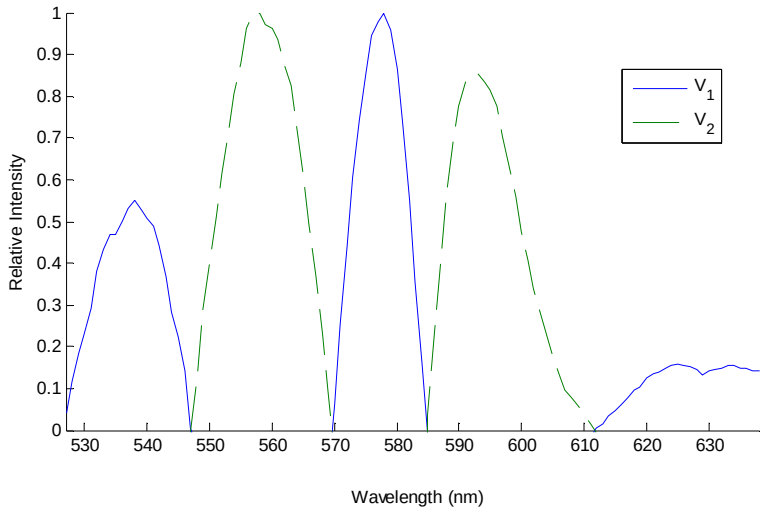

(b)

Figure 5.1 Spectral illuminations used in the 3-shot method for data acquisition. (a) normalized absorbance spectra of oxy and deoxyhemoglobin and (b) the absolute difference between the spectra when one is subtracted from the other

5.2 Data Processing

5.2.1 Calculating Absorbance

According to the Beer-Lambert-Bouguer law, “Equal thickness of an absorbing material will absorb a constant fraction of the energy incident upon it.” Specifically, it relates the radiant

intensity leaving a sample, I, to the radiant intensity incident on a sample, I_0, by an absorbance factor, A, as in equation 5.1.[20]

$$A = \log\left(\frac{I_0}{I}\right) \qquad \text{equation 5.1}$$

Since the DLP® Hyperspectral Imaging system works on the principle of diffuse reflectance, a background cube of the 99.9% reflectance target (spectralon target) is considered to be I_0 or the reference path of light and the sample cube of the area of interest is considered to be *I*. [13] The background cube is saved after initial acquisition and accessed for processing after every sample cube acquisition

5.2.2 Oxyz Deconvolution

The Oxyz deconvolution method utilizes the multivariate least square method to calculate the percent HbO_2 for each pixel. The output bitmap image after processing with the 'Oxyz-Jet' is a color-coded two-dimensional image, where, the more intense pixels (coded as red) signify that the absorbance spectra of that pixel, over the hyperspectral cube, resembles more with the reference spectra of oxyhemoglobin (HbO_2) and hence the less intense pixels (coded as blue) signify that the pixel's absorbance spectrum more closely resembles the reference spectra of deoxyhemoglobin (Hb).

5.2.3 3-Shot Image Analysis

The data cube is proportioned with a background cube with the same parameters taken using the 99.9% reflectance target. This cube represents the absorbance of the broadband illumination at which the image is acquired. Although an absorbance spectra cannot be achieved using this method, the mathematical combination of the three frames will result in an image in which higher pixel values indicate absorbance similar to oxyhemoglobin (HbO_2) and Lower Pixel Values indicate absorbance similar to deoxyhemoglobin (Hb). The captured data cube is 42 times smaller than the spectral sweep (126 shot) data cube and the processing algorithm is simpler. Hence a colored visualization of the change and level of oxygenation can be made much faster using the 3-shot method, making it ideal for live surgical procedures where time is critical. For

plotting $\%HbO_2$ values over time, a 5x5 pixel area is selected in the 3 shot images and a mean and standard deviation is taken for each of the images. For clarity, all images in a run are averaged and the mean and standard deviation for both time and $\%HbO_2$ values are calculated. The runs are then plotted over time.

CHAPTER 6

CLINICAL AND SURGICAL APPLICATIONS

6.1 Human Open Partial Nephrectomies

A total of 26 human surgeries were conducted for this study but only 21 of these cases have been included in the final study due to various reasons stated in table xx.

6.1.1 Assessment of Renal Oxygenation during Open Partial Nephrectomy

6.1.1.1 Introduction

Ischemia time remains the most important factor in determining renal recovery after a partial nephrectomy. Several methods are currently employed to minimize ischemic injury during hilar occlusion (ex. ice slush cooling, artery-only clamping, minimizing clamp time via technique modification),[25,28]; but little is known about the true level of kidney oxygenation before, during, and after the surgical procedure. Amongst other variables, the subsequent re-oxygenation of a kidney after a partial nephrectomy, to a value close to its baseline value, is believed to help prevent post surgical renal recovery. This re-oxygenation is believed to be based on the duration of clamping.

Hyperspectral Imaging (HSI) is a newly applied technology that uses a highly sensitive camera to measure the spectral information of a target to provide various levels of information, including the biochemical changes of tissue during a live surgical procedure. This technology has been used to assess the level of hemoglobin oxygenation in various tissues.[29] By differentiating between the known absorption spectra of oxyhemoglobin and deoxyhemoglobin, the HSI is able to construct a real-time tissue oxygenation map. This technology has also been previously utilized to demonstrate differences in renal parenchymal oxygenation during artery-only and artery-vein hilar clamping in porcine models.[30]

Presently, the baseline renal parenchyma hemoglobin saturation parameters in humans and the dynamic change that occurs during hilar occlusion have not been well studied. The initial experience with HIS, to non-invasively measure renal parenchymal oxyhemoglobin saturation (HbO_2) and determine the kidney's response to hilar occlusion during a partial nephrectomy, has been explained in this research experiment.

6.1.1.2 Materials and Methods

After the initial approval from the Institutional Review Board, HSI was used in consenting patients undergoing open partial nephrectomy (PN) between September 2009 and March 2010. All kidneys were accessed via a flank incision. After the kidney was adequately mobilized and the hilum was isolated, an HSI system was used to take images, the kidney was iced for approximately 7 minutes and the hilum was then clamped using bulldog clamps and subsequent images were acquired, finally the clamp was removed and again subsequent images of the kidney were acquired. Among the 21 cases, both the veins and artery were clamped and in two of the patients, only the artery was clamped.

Previously developed LCTF based Hyperspectral Imaging system and most of the current commercially available HSI systems rely on technology which requires at least 40 seconds to capture process and display the processed images.[29,31] The DLP® (Digital Light Processing, Texas Instruments, Dallas, TX) technology used in the current HSI system reduces the image acquisition and processing time to approximately 20 seconds using a conventional 126 successive band-passes of light.[30] Furthermore, the DLP® hyperspectral system allows a new feature of spectral illumination. The "3-shot mode" that has been developed based on this spectral illumination method has increased the speed of the system to approximately 3-4 frames per second.[29,30]

The DLP® based spectral illuminator (OL490) was used to illuminate the kidney from a fixed distance with known spectra of wavelengths between 520nm and 645nm.[30] These spectra incorporate the reflectance (or apparent absorbance) of both oxyhemoglobin and deoxyhemoglobin. Reflectance images were then captured by a charge-coupled device (CCD)

focal plane array. Collected data were then deconvoluted to assess numerical percentage of oxy-hemoglobin values (%HbO_2) and the resulting chemically relevant data were color-encoded, with various colors representing the relative %HbO_2 as seen in figure 6.1.[29,31] . The relative percent contribution of both oxy and deoxyhemoglobin was determined via the hyperspectral imaging system over an “optical biopsy” area consisting of a 5x5 pixel square.

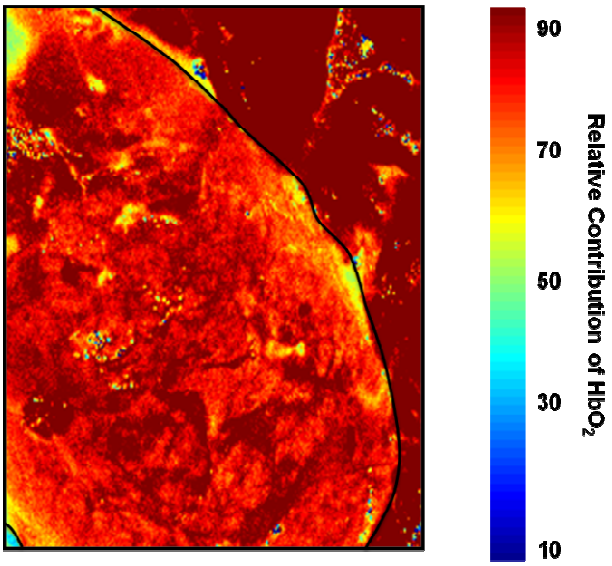

Figure 6.1: Renal hemoglobin oxygenation as observed on HSI prior to clamping (kidney outlined in black)

6.1.1.3 Results

The kidneys of twenty one patients were imaged with HSI [mean age 55, (29-77)] while undergoing open PN with ice slush cooling for 7 to 10 minutes prior to tumor excision. Mean tumor size was 3.3 cm and clamp time was 36.8 minutes (23 to 49). Patient demographics are as listed in Table 6.1. All kidneys demonstrated high HbO_2 saturation during pre-clamp imaging with a median of 74.63% which corresponds to a bright red color on a color-mimetric scale as depicted in figure 6.1. HSI demonstrated a median 20.0 percent decrease in %HbO_2 from baseline after a median 9.5 minutes of hilar occlusion as shown in figure 6.2.

Table 6.1 Patient demographics

		Mean (range)
Age		55.2 yrs (29-75)
Tumor Size		3.3 cm (1.6-4.5 cm)
Ischemia Time		36.8 min (23-49 min)
EBL		261.3 ml (30-800 ml)
		N= (%)
Gender:	Male	12 (63%)
	Female	7 (37%)
Race:	African American	2 (11%)
	Caucasian/Other	17 (89%)
Pathology:	Clear Cell	12 (63%)
	Papillary	4 (21%)
	Other	3 (16%)

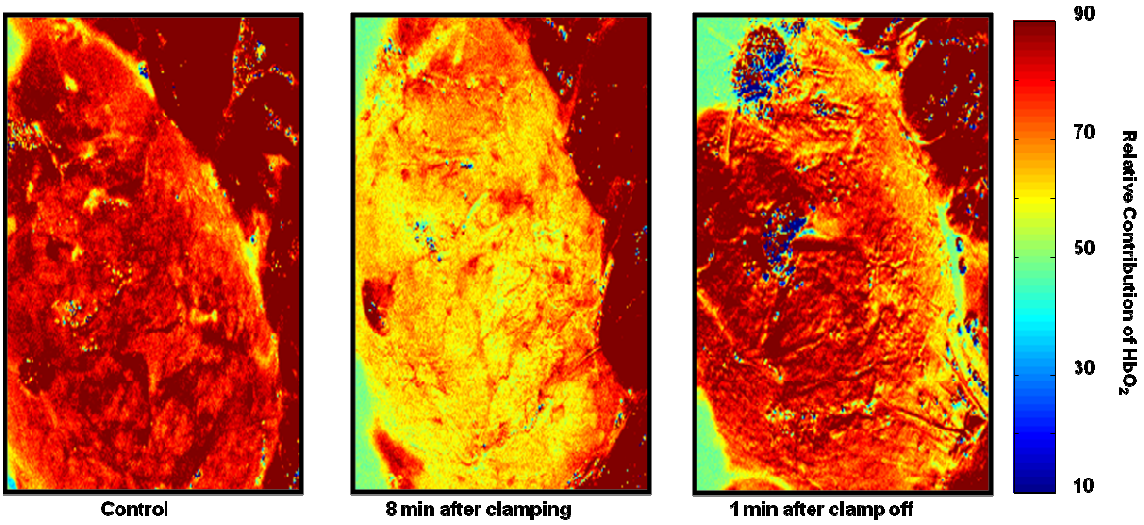

Figure 6.2 : Hyperspectral images demonstrating changes in oxyhemoglobin saturation at different stages during a partial nephrectomy

Interestingly, the $\%HbO_2$ rebounded to levels between 80 and 90 percent of baseline after the initial drop to 80% as depicted in the normalized plots in figure 6.3. It plateaued at this level for the duration of the clamp time. Detailed oxygenation parameters are listed in Table 6.2. The trend line in figure 6.2 is a 6^{th} order polynomial fit with an R^2 value of 0.64 and this may not indicate an exact trend. A more accurate fit can be achieved with data on more subjects

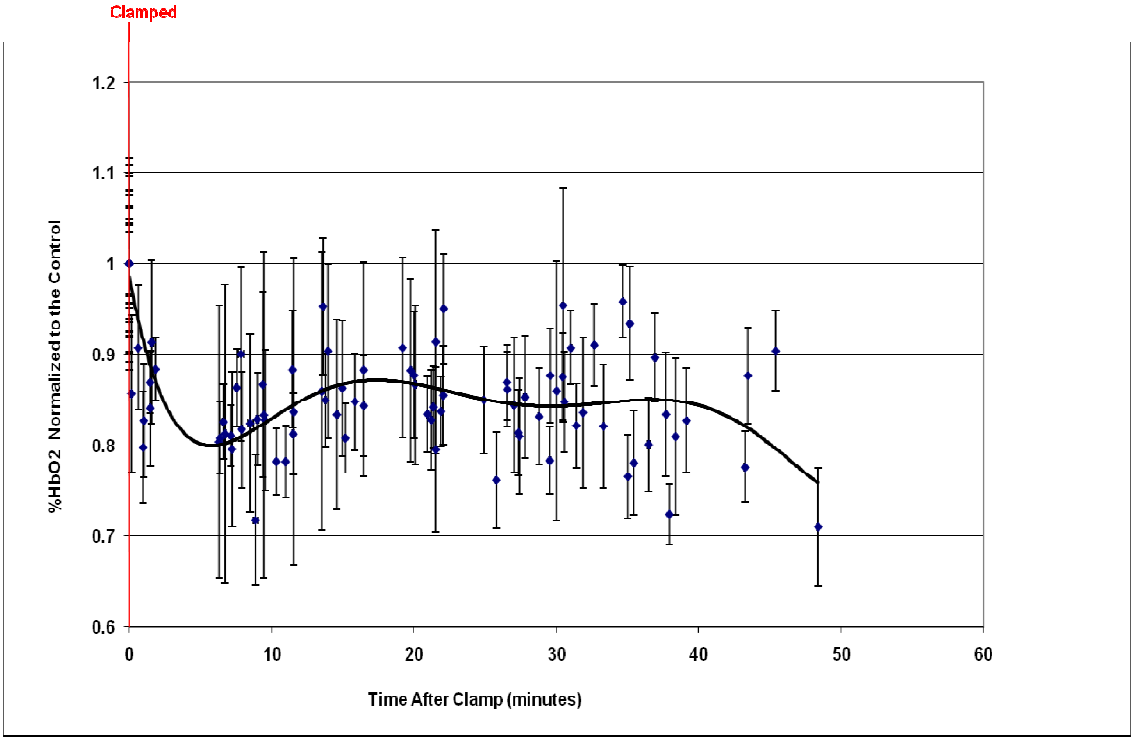

Figure 6.3 Normalized values of renal percentage HbO_2 values during hilar occlusion

Table 6.2 Renal oxygenation parameters

	Mean	Median	Range
Baseline %HbO_2	73.97	74.63	58.49 - 84.65
Nadir HbO_2 after clamping (ratio of baseline HbO_2)	0.81	0.80	0.76 – 0.94
Time to Nadir (after clamp) (min)	17.7	9.5	0.9 - 48.4
HbO_2 after unclamping (ratio of baseline HbO_2)	0.99	0.99	0.84 - 1.22
Time to return to baseline HbO_2 after unclamping (min)	7.9	5.8	0.2 - 22.1

Upon clamp removal, the %HbO_2 returned to baseline indicating a complete reperfusion at a median of 5.8 minutes after unclamping. Figure 6.2 illustrates the change in color associated with decreased %$Hb0_2$ during hilar occlusion. The corresponding mean %$Hb0_2$ at several time

periods during hilar occlusion are shown in figure 6.3. Similarly, the mean %HbO_2 after renal perfusion was re-established as shown in figure 6.4. The trend line in figure 6.4 is a 3rd order polynomial fit with an R^2 value of 0.36 and this may not indicate an exact trend. A more accurate fit can be achieved with data on more subjects

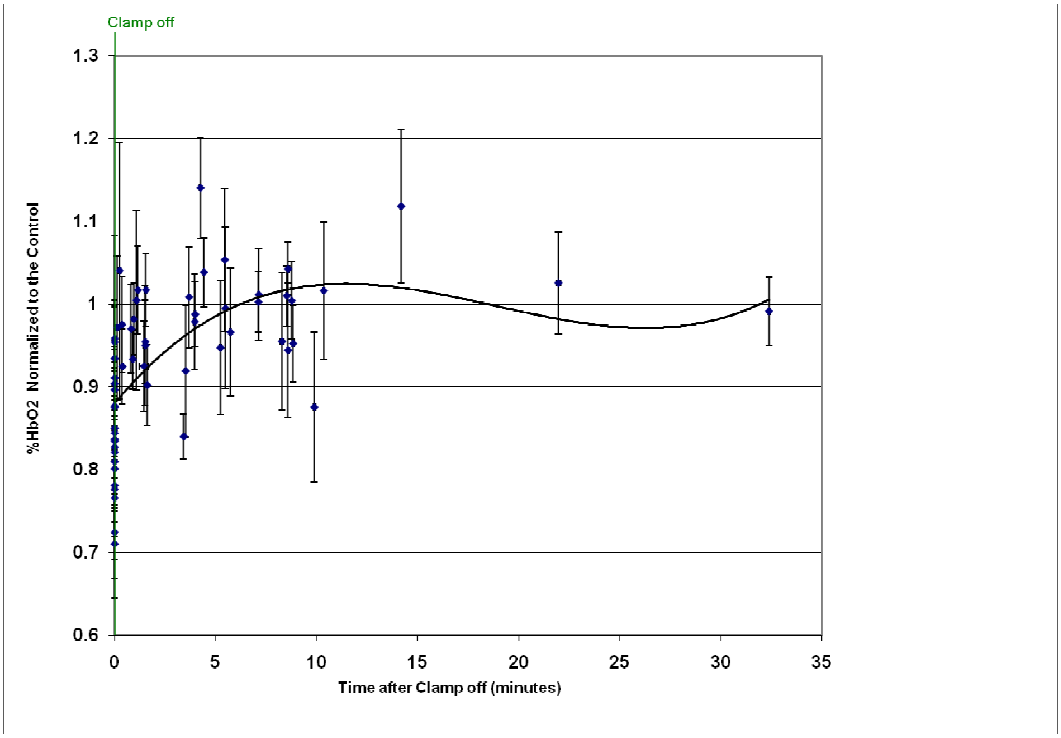

Figure 6.4 Normalized renal percentage HbO_2 values after unclamping

6.1.1.4 Discussion

Preservation of renal function during partial nephrectomy is an important aspect to predict post surgical recovery of the kidney, and much attention has been focused on the impact of ischemia time on post-operative renal function.[34,35] Most reports estimate safe warm and cold ischemia times to be around 30 minutes before renal function is compromised. In the largest retrospective evaluation of solitary kidneys published, Thompson et al found that warm ischemia time longer than 20 minutes or cold ischemia time longer than 35 minutes increased the chances of renal insufficiency.[35] Despite this knowledge, there are still patient- and surgery-specific

variables such as the potential for microvascular disease and differences in baseline perfusion that are not accounted for and, until now, have been difficult to assess. HSI can be an important tool in this regard, as a non-invasive means to measure differences in renal oxygenation and perfusion in individual patients. Such knowledge of the metabolic state of the kidney during hilar occlusion is fundamental to understanding renal ischemia and its correlation with renal insufficiency. DLP® hyperspectral imaging may be a novel modality to perform such assessments as it is fast and non-invasive with applications in both open and laparoscopic surgery.[9]

Recently, Crane et al have demonstrated the utility of a similar technique termed optical enhancement as a means to identify vascular structures and assess tissue oxygenation in both laparoscopic donor nephrectomy and partial nephrectomy.[31,32] Their deconvolution of images captured with a conventional CCD camera intra-operatively demonstrated a qualitative assessment of changes in oxygenation during hilar occlusion. Mean region of interest arbitrary units were collected and then converted to estimated oxygen saturation values post-operatively using a formula derived from pig calibration studies.[32] This technique does not use specific wavelength illumination to determine numerical hemoglobin saturation values.

We have previously utilized HSI technology as a means to compare renal hemoglobin saturation changes between artery and vein and artery-only clamping in the porcine model.[30] This experience demonstrated that renal tissue oxygenation drops rapidly after occlusion of the renal vasculature (to approximately 66% of baseline in the pig) and returns to near baseline 30 minutes after reperfusion. However, baseline renal parenchyma hemoglobin saturation parameters in humans and the dynamic change that occurs during hilar occlusion have not been well studied. Our data indicate that renal hemoglobin saturation in the human kidney is relatively uniform and that during hilar occlusion it drops precipitously by 20%, reaching a nadir during the initial standard ice slush exposure time. It then recovers to between 80-90% of baseline and remains remarkably stable. This observation suggests that beyond 10 minutes of ischemia oxygen disassociation from the hemoglobin molecule has reached equilibrium with no additional oxygen delivery to the kidney parenchyma.

To better understand these observations it is important to emphasize two points. First, the mechanism of measurement of tissue HbO_2 via HSI is unlike conventional pulse oximetry in that HSI measures the concentration of fully oxygenated hemoglobin compared to fully deoxygenated hemoglobin at the surface parenchyma (microvascular) level. As a result, the value is not equivalent to an arterial oxygen saturation value that would be depicted by pulse oximetry. Second, the oxygen binding kinetics of hemoglobin is also involved. As oxygen tension decreases (as in the case of hilar renal ischemia), the oxygen binding affinity of hemoglobin strengthens. (shown in the oxygen dissociation curve in figure 6.5). The P50 of human hemoglobin occurs at a PO2 of 26mm Hg. In other words, the partial pressure of oxygen would need to be 26 mm Hg before the oxyhemoglobin values decreased to 50% of baseline. Accordingly, it likely requires a significant duration of ischemia and tissue oxygen demand to cause the hemoglobin molecule to release its entire oxygen stores. Short ischemia times coupled with decreased oxygen demand via ice slush cooling may limit renal HbO_2 saturation from dropping further during standard operative times. Prior animal experiments have demonstrated that even at one hour of hilar occlusion, tissue $\%HbO_2$ still remains at approximately 67% of baseline.[30]

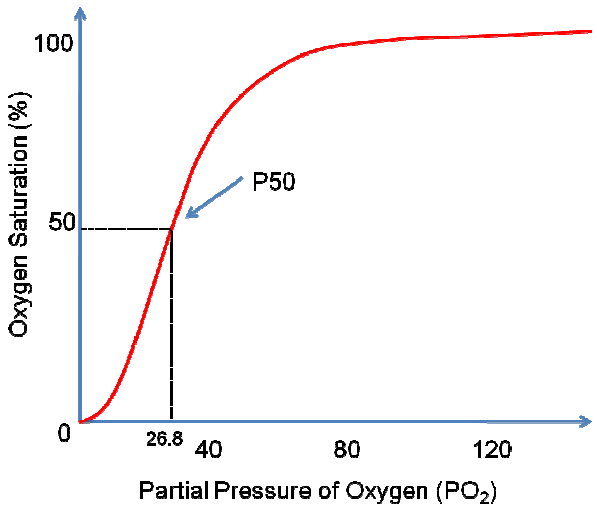

Figure 6.5 Oxygen disassociation curve

One confounding variable that may clinically prevent a larger drop in $\%HbO_2$ is that the kidney may maintain some degree of unrecognized perfusion during hilar occlusion. This is often apparent during tumor excision, as transected vessels can bleed, suggesting vascular flow despite presumed complete hilar control. This finding may help explain our observation that the $\%HbO_2$ appears to recover somewhat during the clamp period. Future work will aim to elucidate the meaning of these experimental findings. In addition, as a pilot investigation, our patient population was not standardized. While the majority of patients underwent artery and vein occlusion, 2 (11%) underwent artery only occlusion. While numerous studies have indicated a benefit is preserving renal function [25] and oxygenation [30] with artery-only clamping, our study is not powered adequately to detect such a benefit in humans. As our study population increases, the data may allow for such observations.

6.1.1.5 Conclusions

DLP® HSI serves as a fast, non-invasive method to assess renal microvascular HbO_2 saturation intraoperatively. Nadir $\%HbO_2$ levels are clinically reached within 10 minutes of initiation of cold ischemia and return to baseline rapidly after hilar flow is reestablished. This knowledge may allow for future surgical or pharmacologic interventions that maintain some degree of renal perfusion and oxygenation using real time assessment of $\%HbO_2$ levels. In addition, such non-invasive, real-time imaging may help identify which kidneys may be at greater risk for ischemic damage and tailor the surgery appropriately.

6.1.2 Baseline Percent Oxyhemoglobin Values as a Prediction of Post Operative Renal Function

6.1.2.1 Introduction

Although ischemia time has been a primary concern in protecting post operative renal functions during partial nephrectomies,[25,28] there are many other factors that can affect it, such as pre-existing medical conditions of patients and hence the condition of the kidney before the operation. A patient brought in for surgery can have pre-existing medical conditions that can largely contribute to post surgical recovery. One such case could be that the patient is suffering from arterial thrombosis and hence the kidney is robbed of its proper blood supply, predisposing

the patient to lose proper renal functionality after a surgerical procedure. Hyperspectral Imaging being a non-invasive technique provides a real-time oxygenation map of tissue during the actual procedure and it is hypothesized that the system can selectively predict post operative renal function recovery based on baseline tissue oxygenation.[45]

6.1.2.2 Materials and Methods

As the previous experiment, data from 21 human patients [mean age 57, (range 29-78)] was used for this study. After the initial approval from the Institutional Review Board, HSI was used in consenting patients undergoing open partial nephrectomy (PN) between September 2009 and March 2010. All kidneys were accessed via a flank incision. After the kidney was adequately mobilized and the hilum was isolated, an HSI system was used to take images, the kidney was iced for approximately 7 minutes and then the hilum was then clamped using bulldog clamps and subsequent images were taken, finally the clamp was removed and subsequent images of the kidney were taken. Among the 21 cases, both the veins and artery was clamped for 19 patients and only the artery was clamped in the remaining two cases. Patients were categorized as high (greater than 75%HbO_2) or low (less than 75%HbO_2) oxygenation based on their oxygenation values during baseline (control). A post-operative estimated glomerular filtration rate eGFR was assessed, as a renal function test, on these groups and the results were compared with the baseline tissue oxygenation values from the hyperspectral imaging system.

6.1.2.3 Results

From the total 21 human cases, 7 patients with higher %HbO_2 values during control were grouped as the 80ish and 14 patients with low %HbO_2 values during control were placed in the 70ish group; as the mean %HbO_2 value during baseline for the 80ish group was 78.7616 ± 3.1795 and the mean %HbO_2 value during control for the 70ish group was 69.2102 ± 5.1778. The plots for the two cases are as shown in figure 6.6. The trend lines in figure 6.6 for both the cases are 3rd order polynomial fits. This may not indicate an exact trend for both the cases and a more accurate fit can be achieved with data on more subjects. However, it is evident from the plots that both the groups follow a very similar trend and the 70ish group seems to dip lower compared to

the 80ish group. The nadir (minimum point for the 70ish group was found to be (46.555±4.989) %HbO_2 at (7.217±0.050) minutes after clamping and the nadir for the 80ish group was found to be (59.990±2.974) %HbO_2 at (10.983±0.032) minutes after clamping.

There was no difference in tumor size (p=0.22), hematocrit (p=0.93), clamp time (p=0.83), or pre-op eGFR (p=0.78) between the two groups. Using creatinine values obtained post-operative day 1 or 2, it was determined that the median peri-operative change in eGFR in the high HbO_2 group was -3.5, while it was -14.8 in the low HbO_2 group (p=0.037). This difference was resolved by 3 months.

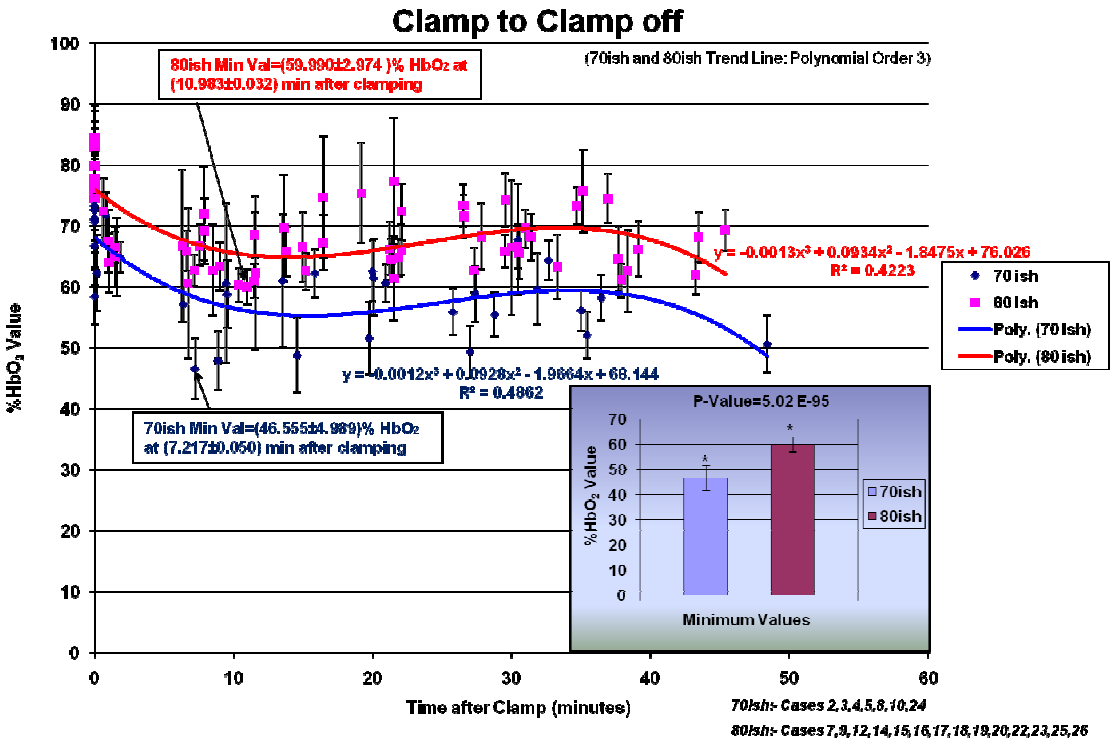

Figure 6.6 Clamp to clamp off values for cases separated into 70ish and 80ish %HbO_2 values during control (baseline)

The results from these tests suggests that groups with lower % HbO_2 values at control (70ish group) as suggested by the hyperspectral imaging system correlated to lower post

operative renal functions compared to the group with higher $\%HbO_2$ values at control (80ish group).

6.1.2.4 Discussion

Although the hyperspectral imaging system had been previously used to compare $\%HbO_2$ value changes for 'artery only' vs. 'artery and vein' occlusion [30], a study on the overall affect of baseline values of $\%HbO_2$ on post operative renal function recovery had not been conducted. This study suggests that different patients can have varied pre-operative kidney functions. A low $\%HbO_2$ value during control could also be indicative of pre existing medical conditions such as a Thrombosis wherein, the kidney is not well perfused and hence devoid of the necessary oxygen required for it to maintain proper kidney functions. Patients with such conditions could be at higher risks of post-operative renal failure. Abstract on this work won first prize at the World Congress of Endourology meeting. [45]

6.1.2.5 Conclusion

The human cases were separated into two groups (70ish and 80ish) based on the $\%HbO_2$ values during control (baseline). A post operative renal functional analysis was conducted on these patients. Results show that patients with higher $\%HbO_2$ values during control (80ish group) have better post operative renal functions compared to the cases with lower $\%HbO_2$ values at control (70ish group). The hyperspectral imaging system can hence be used to provide an immediate feedback to surgeons to make correct judgments and help in the decision making process during a surgery to ensure the best post-surgical recovery.

6.2 Porcine Open Partial Nephrectomies

6.2.1 Renal Function Analysis for Different Levels of Clamping using Transonic Flow Unit and Hyperspectral Imager

6.2.1.1 Introduction

While partial nephrectomy preserves renal function compared to radical nephrectomy, it typically involves temporary occlusion of the renal vasculature in order to reduce bleeding and preserve visualization of tissue planes. The resulting ischemia can itself damage nephrons in a

time-dependent process that is incompletely understood. Several technical modifications including application of ice slush to the renal parenchyma, artery-only clamping, and administration of agents such as mannitol have been proposed and adopted as methods to try to reduce ischemic injury.

Previous investigations at UTSW found that partial arterial occlusion protects renal function and oxygenation in a porcine model, which may be due to a modest oxygenation from venous backflow.[36,37]., Thus, it is hypothesized that partial arterial clamping, wherein some degree of flow is preserved during tumor resection, might also mitigate ischemic injury. These studies were limited in that tissue oxygenation was measured at only a single location in the kidney using an obtrusive and invasive probe. In addition, the degree of blood flow preserved during surgery was not well quantified. As a result, a novel hyperspectral imaging (HSI) technique that non-invasively monitors renal oxyhemoglobin during partial nephrectomy was found to accurately confirm that artery-only clamping improves renal oxygenation relative to hilar occlusion.[30] HSI uses a programmable DLP® spectral illuminator and a highly sensitive camera to detect the visible wavelengths of light for measuring spectral properties of oxy- and deoxyhemoglobin to generate a real-time tissue oxygenation/perfusion "map." [30] In this investigation, we sought to determine if incomplete renal artery (RA) occlusion is reno-protective in a porcine model; and if so, is this protective effect, when monitored, explained by differences in tissue oxygenation detectable by HSI over time.

6.2.1.2 Methods

Study Design

The study was conducted following approval by the institutional animal care and use committee at UTSW. Fourteen female farm pigs (mean weight 32kg, range 22-50kg) were included in this study and underwent 2 surgical procedures. A laparoscopic nephrectomy was performed to create a solitary kidney model. Following a 7-day recovery period, a contralateral open lower pole partial nephrectomy was performed to further reduce the parenchymal reserve. Animals were then euthanized after a blood draw 7 days after partial nephrectomy. Surface

parenchymal cooling was not employed in any of the cases. Intraoperative hemodynamics (blood pressure, heart rate, core temperature, and pulse oximetry) were monitored and maintained consistent during all procedures. Two sample t-tests were used to compare data between groups.

As previously described, the DLP®(Digital Light Processing, Texas Instruments, Dallas, TX) HSI camera illuminates the kidney with a known spectra of wavelengths between 520nm and 645nm.[30] These spectra were selected because they incorporate the reflectance values of both oxyhemoglobin and deoxyhemoglobin. The images are captured by a charge-coupled device (CCD) focal plane array and the data are formatted into a 3-dimensional hyperspectra image cube consisting of a spectral wavelength dimension and two spatial image dimensions.[29] The relative percent contribution of oxyhemoglobin perfusing the kidney tissue is visualized using a novel DLP® hyperspectral imaging system as an "oxygenation map" created by assigning different colors to the varying percentage of oxyhemoglobin.[38]

6.2.1.3 Operative Procedures

A right open partial nephrectomy was performed through an extraperitoneal flank incision. The kidney was mobilized with careful dissection of the renal artery. In all cases, only a single renal artery was identified. Following mobilization, an ultrasonic flow probe (Transonic Systems, Ithaca, NY) was placed around the renal artery as shown in figure 6.6 and the baseline renal flow was recorded. A purpose-built, stainless steel adjustable vascular clamp was then placed distal to the flow probe and "dialed down" to a tightness that reduced the blood flowing into the kidney to the percentage of an unocclude renal artery as determined by the ultrasonic flow probe(i.e. 0% blood flow [100% clamping], 10% blood flow [90% clamping], 25% blood flow [75% clamping]). Performing a lower pole partial nephrectomy with a 50% RA occlusion was found to result in excessive bleeding unacceptable for in the human setting and thus this study focused on 25%, 10%, and 0% RA blood flow.

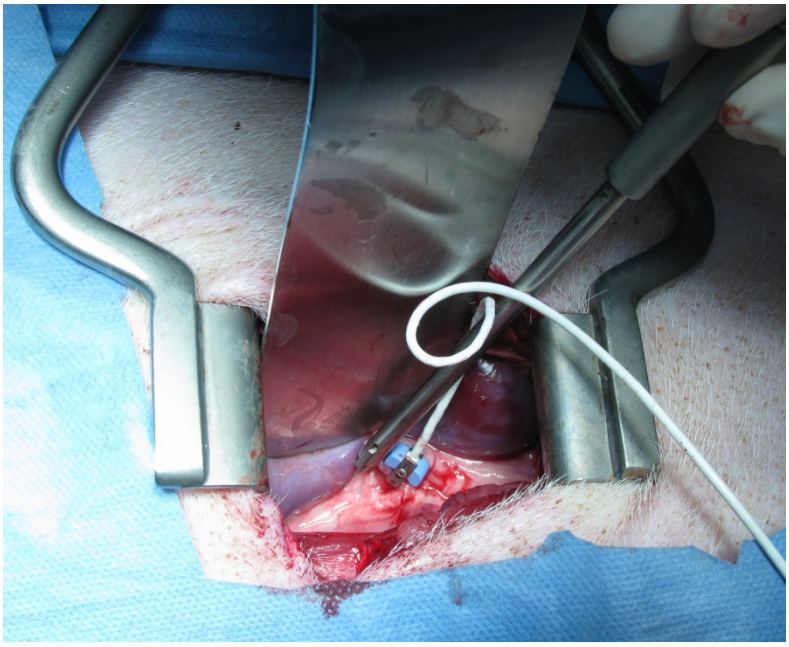

Figure 6.7 Intra-operative view during open partial nephrectomy. The kidney is being retracted to show flow probe (blue) and the adjustable clamp (stainless steel) in place across the renal artery.

The blood flow was maintained at the assigned level for 60 minutes since prior research has demonstrated pigs universally experience a temporary renal insult after this period of ischemia.[6] Prior investigations have also demonstrated the nadir oxygenation level to be reached during this time frame, regardless of variations in vascular clamping.[30,36,37] Hyperspectral images were taken just prior to clamping, every 5 minutes during the ischemic period and for 20 minutes after the clamp was removed. Thirty minutes after the clamp was initially applied, a lower pole partial nephrectomy ((approximately 20% of the total kidney length removed) was performed. The base of the resection was oversewn with 2-0 Vicryl suture for hemostasis and to close any defects in the collecting system and the parenchyma was closed with interrupted sutures over an absorbable hemostatic bolster. After 60 minutes had elapsed, the clamp was removed and the blood flow as measured by the flow probe was recorded over a mean of 30 seconds at an average of 6 minutes after clamp removal.

6.2.1.4 Results

Open partial nephrectomy was performed on all animals a week later as planned. Comparison of renal artery flow (as measured by the ultrasonic flow probe) showed similar baseline flow rates amongst all 3 groups as indicated by the P-values in Table 6.3.

Table 6.3: Arterial flow as measured by the ultrasonic flow probe.

	0% Renal Artery Flow	10% Renal Artery Flow	25% Renal Artery Flow	P value (0% vs 10% flow)	P value (0% vs 25% flow)	P value (10% vs 25% flow)
Number of animals	5	4*	5			
Mean baseline flow , ml/min (range)	258 (based on 4 animals) (147-323)	224 (125-368)	231 (171-318)	0.65	0.63	0.92
Mean flow during clamp, ml/min (range)	0 (0)	20 (15-33)	55 (40-75)	0.02	0.002	0.006
				P value comparing baseline to post-clamp removal flow		
				0% clamped	10% clamped	25% clamped
Mean flow after clamp removed, ml/min (range)	125 (based on 3 animals) (85-136)	170 (90-230)	192 (based on 3 animals) (97-260)	0.15	0.46	0.61

As expected in a controlled variable, the RA flow during the clamping period differed significantly between groups. In the first 10 minutes after the removal of the clamp RA flow recovered fully in all 3 groups

Hyperspectral imaging was found to be a very sensitive tool for detecting differences among the 3 groups. The baseline $\%HbO_2$ was equivalent in all the cohorts as shown in table 6.4. As expected, restricting the blood flow resulted in decreasing tissue oxygenation .The nadir $\%HbO_2$ (i.e. the lowest recorded $\%HbO_2$) in the 0% RA flow group was statistically lower than that seen in both the 25% and 10% flow groups ($p=0.01$ and 0.04, respectively). The rate of deoxygenation (drop in $\%HbO_2$) from baseline to nadir was similar during 0% and 10% RA flow;

however, restricting the RA flow to 25% was found to increase the deoxygenation time to 37 minutes. With the return of tissue perfusion upon removal of the clamp, the $\%HbO_2$ rapidly returned to baseline in all three groups as shown in the trend of figure 6.7 and the images in figure 6.8. As explained in earlier experiments, the trend lines for the different cases in figure 6.7 are polynomial fits and may not indicate the exact trends. More data can be collected to verify the correct trend lines. However, the trends seem to show a similar nature (a slight recovery after an initial drop) in the human cases as well. This could be an actual physiological occurrence and might be indicative of changes in chemicals such as lactic acid or other metabolites such as Uric acid, phospholipids; but further research is required to verify this behavior.

Table 6.4: Tissue oxygenation, $\%HbO_2$, as a measure of the DLP® Hyperspectral Imager.

	0% Renal Artery Flow	10% Renal Artery Flow	25% Renal Artery Flow	P value (0% vs 10% flow)	P value (0% vs 25% flow)	P value (10% vs 25% flow)
n	5	4	5			
$\%HbO_2$ Baseline	77.7±5.7	74.2±2.8	75.0±3.2	0.28	0.40	0.71
$\%HbO_2$ After 10 min of clamping	53.6±1.6	58.0±2.4	69.7±5.1	0.04	0.001	0.004
$\%HbO_2$ at Nadir	52.9±2.2	57.0±2.5	65.6±7.1	0.04	0.01	0.05
$\%HbO_2$ After clamp removal	75.1±7.4	77.9±5.1	78.6±5.6	0.53	0.43	0.85

After removing the clamp from the renal artery the average percentage of HbO_2 of all three groups returned to a baseline average value of 77.18 ± 1.82 $\%HbO_2$, which is within error of the pre-clamp baseline measure of 75.63 ± 1.81 $\%HbO_2$.

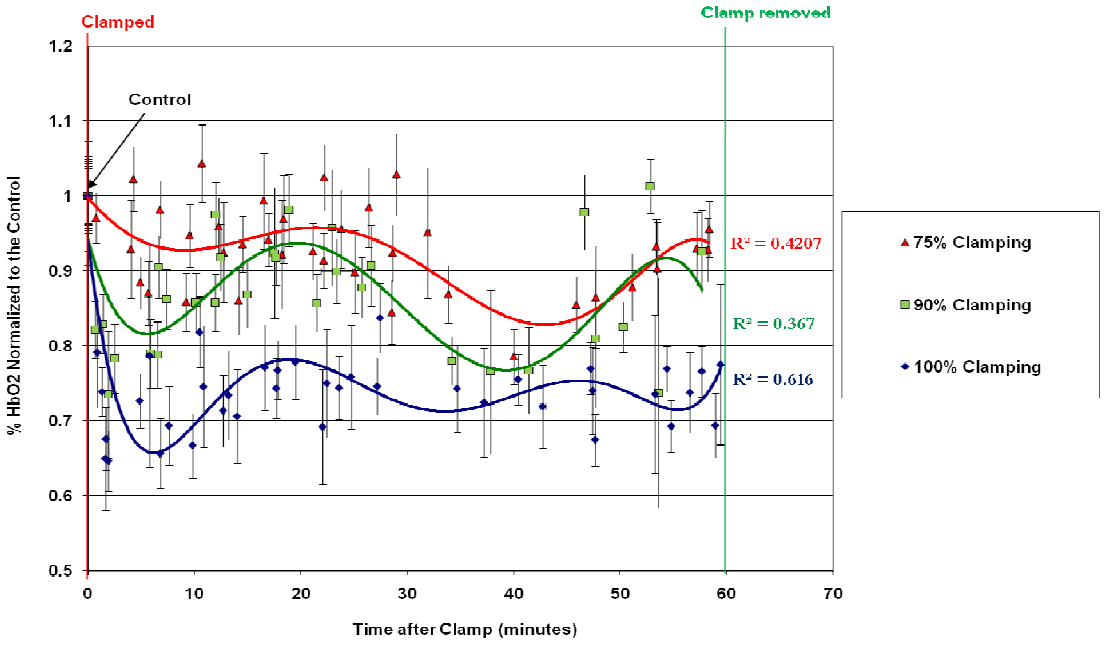

Figure 6.8 images the kidney tissue deoxygenation occuring during clamping that is visualized by the yellower pixels of the middle column images, the nadir condition. The figure clearly shows the higher level of oxygenation at the nadir condition in the 25% RA flow group since the kidney appears more orange than the kidneys in the 10% and 0% flow groups.

Since we utilized a porcine model, we were unable to estimate GFR and therefore used serum creatinine (SCr) drawn at 3 different points to measure the impact of partial RA flow on renal function (Table 3). Because a laparoscopic nephrectomy was performed to create a solitary kidney model, a new "baseline" SCr was established just prior to the partial nephrectomy. Interestingly, despite equivalent care prior to partial nephrectomy, the pigs in the 25% RA flow group had a statistically higher baseline SCr than those in the 0% flow group (p=0.046). Since these baselines differed slightly, the impact of partial renal artery flow was evaluated comparing the changes in SCr (ΔSCr) between groups from baseline to those drawn on) post operative day (POD) 3 and 7.

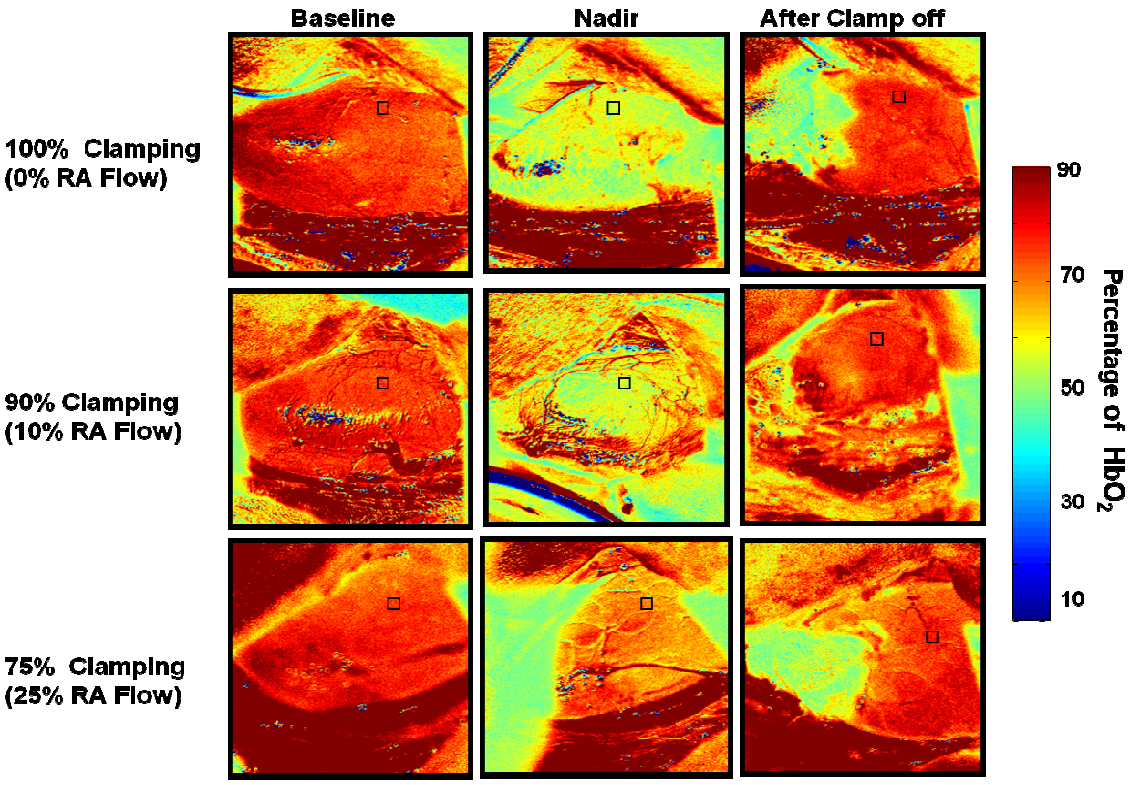

Figure 6.9 Hyperspectral images of the kidneys in three different cases with varied renal arterial (RA) flow. Nadir is the image with minimum $\%HbO_2$ value with 10 minutes of clamping for all cases. (*100% Clamping - Case 16 (C302) runs 1, 3, 12 , 90% Clamping - Case 5 (C288) runs 1, 2, 12 , 75% Clamping – Case 11 (J9) runs 1, 2, 12)*

While there was no difference in ΔSCr seen between groups on POD3, by POD7 the change in renal function was found to favor 25% renal artery flow ($p < 0.05$; Figures 6.9 and 6.10). Specifically, the ΔSCr was 0.42, 0.38 and 0.16 mg/dl when measured on the seventh postoperative day for 0%, 10% and 25% RA flow respectively. The improved parenchymal oxygenation ($\%HbO_2$) demonstrated intraoperatively by HSI predicted the smaller change in SCr measured 7 days postoperatively in the 25% RA flow group.

While the ultrasonic flow probe proved to be a very sensitive and useful tool for measuring blood flow in an experimental non-invasive fashion, we found that the relatively large footprint of the probe (approximately 9 x 6 mm) made it difficult to use, particularly when the porcine renal artery was small. In a few cases we found it to be unsafe or impossible to place

both the clamp and the flow probe on the renal artery. In these cases, the pig was assigned to the complete occlusion (0% RA flow) group since we were unable to measure the appropriate partial flow rates. Similarly, removal of the clamp while leaving the flow probe in place was challenging. If the probe inadvertently came off with the clamp, we prioritized obtaining HSI images expeditiously and did not delay imaging by taking the time to replace the flow probe. We therefore do not have complete post-occlusion flow rate data from all cases.

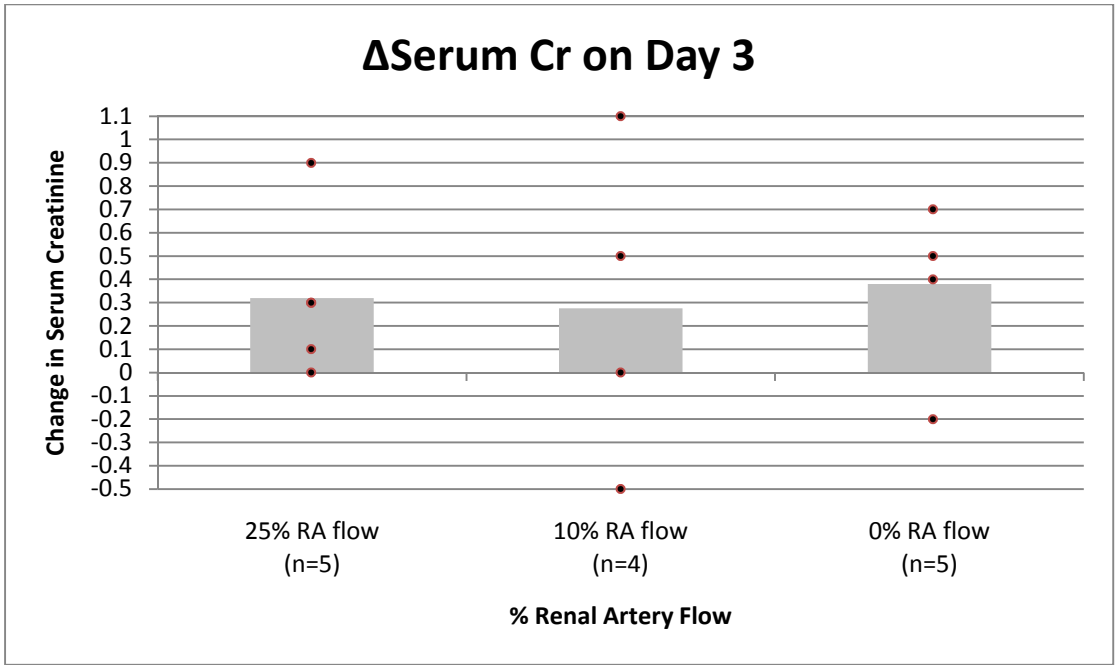

Figure 6.10 Change in serum creatinine between baseline and **Day 3.** The bars in both figures demonstrate the mean ΔSCr while the dots represent individual data points (duplicate results are represented by a single dot). There was no statistically significant difference between any of the groups.

Table 6.5: Mean creatinine data (mg/dL) with Ranges.

	0% Renal Artery Flow	10% Renal Artery Flow	25% Renal Artery Flow	P value (0% vs 10% flow)	P value (0% vs 25% flow)	P value (10% vs 25% flow)
Preoperative	1.5 (1.3-1.7)	1.775 (1.6-2.2)	1.84 (1.5-2.4)	0.125	0.046	0.410
Post op Day 3	1.88 (1.4-2.4)	2.05 (1.6-2.7)	2.16 (1.7-2.7)	0.287	0.154	0.369
Change from Day 0	0.38	0.275	0.32	0.386	0.395	0.451
Post of Day 7	1.92 (1.7-2.2)	2.15 (1.5-2.8)	2.00 (1.7-2.3)	0.226	0.318	0.317
Change from Day 0	0.42	0.375	0.16	0.393	0.048	0.076

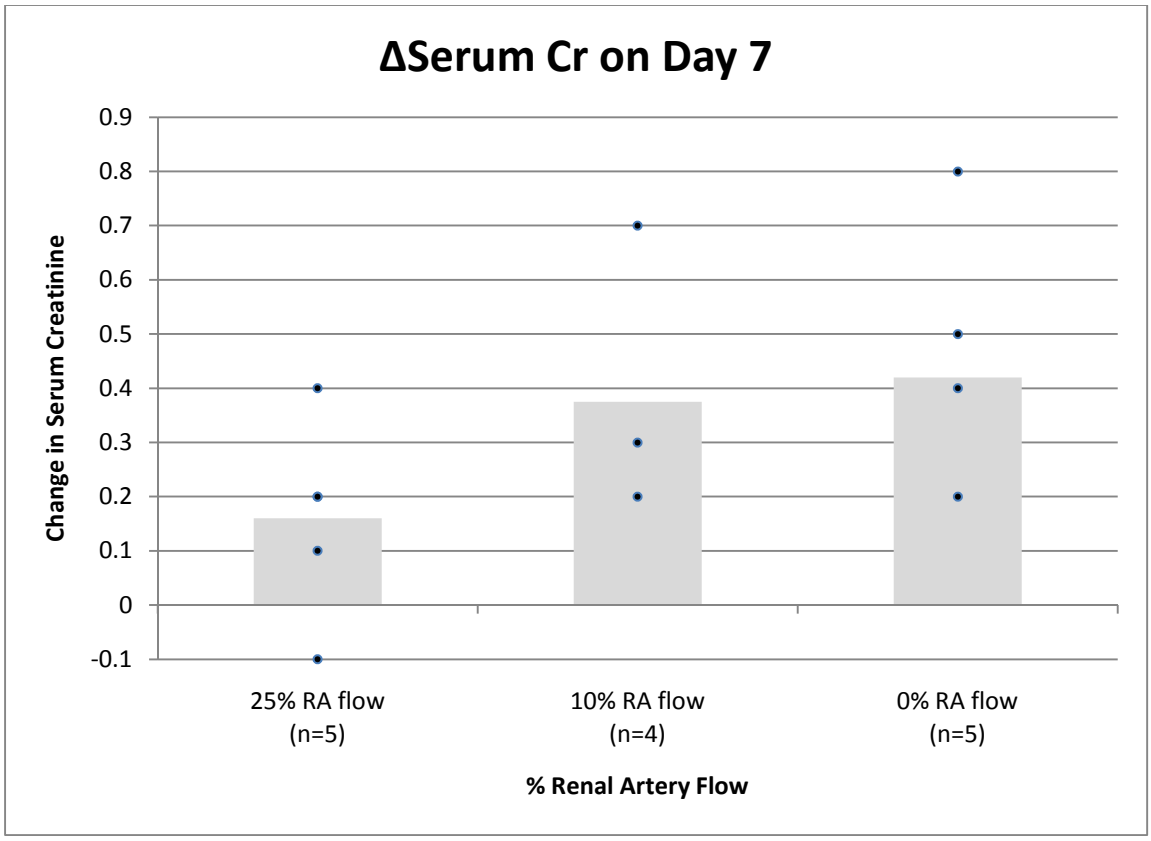

Figure 6.11 Change in serum creatinine between baseline and **Day 7.** The mean ΔSCr in the 25% RA flow group was lower than that of the 0% flow group (0.16 vs 0.42, p=0.048).

6.2.1.5 Discussion

Partial nephrectomy has become the gold standard therapy for small renal masses as it preserves nephrons and renal function while providing similar cancer control to nephrectomy.[40,41] During the procedure the renal hilar vasculature is typically clamped to improve visualization and minimize bleeding. This vascular occlusion, however, is itself damaging to kidney function. A variety of measures have been employed to attempt to reduce the damage from this ischemic period. One of the most common tactics is to use ice slush cooling Another surgical maneuver that can decrease functional impairment is to clamp the renal artery alone, rather than both the vein and artery.[25] This is thought to provide retrograde venous perfusion of the kidney as well as allow efflux of toxic metabolites. Other reno-protective strategies involve the administration of pharmacologic agents such as mannitol in an attempt to minimize ischemic renal damage.[42]

Despite these manipulations, ischemic injury may still occur and there remains interest in other measures to reduce injury and extend the ischemia time during partial nephrectomy. In a porcine model, Raman and coworkers compared post-operative creatinine changes in pigs who underwent either complete or partial (approximately 50%) occlusion of the renal artery while measuring tissue oxygen partial pressures (PO2) with a a needle-like probe (Licox probe, Integra, San Diego, CA) inserted into the kidney.[37] They found that partially clamping the renal artery resulted in a prolongation of the time to reach the nadir PO2 compared to total clamping (23.1 vs 8.7 minutes) and also resulted in improved post-operative renal function, as measured by serum creatinine a week after surgery. However, this investigation was limited in that the renal artery flow was not accurately measured.

A recent study in a porcine model employed hyperspectral imaging (HSI) to demonstrate that artery-only occlusion preserved renal parenchymal oxygenation longer than clamping of both the artery and vein.[30] HSI technology uses principles of spectroscopy and implementing DLP® based imaging technology for color encoding the quantity of oxyhemoglobin at each image detector pixel in real time at near video rates.[9,14.30,38,43] Using this technology, Tracy and

colleagues found that there was a significantly higher oxygenation in the artery-only group during the first 36 minutes of clamping.[30] Crane and associates have recently used similar technology to demonstrate decreasing porcine renal oxygenation with reductions in fractions of inspired oxygenation and decreased perfusion during hilar clamping in human laparoscopic partial nephrectomy patients.[32,44] In the current study, we combined techniques from our previous work, utilizing both the concept of partial renal artery clamping as well as the non-invasive determination of tissue oxygenation with HSI. Specifically we quantified renal artery flow using an ultrasonic flow probe and utilized a custom-built titrateable vascular clamp such that renal artery flow could be set to a specific percentage of baseline. Utilization of HSI technology to replace a cumbersome and invasive needle PO_2 probe allowed for a practical, non-contact technique to measure tissue oxygenation (%HbO_2). This study confirms that marginal preservation of renal blood flow and consequently oxygenation as demonstrated by HSI, results in improved post-operative renal function. The sensitivity of HSI demonstrated that even small variations in the renal blood flow (10%) can result in significant differences in oxyhemoglobin delivery to the kidney. The improvement in overall tissue oxygenation as well as the prolonged time to nadir %HbO_2 compared to the 0% and 10% RA flow groups likely explains the reno-protective effect seen in 25% RA flow. In addition, we hypothesize that a small degree of constant blood flow during partial nephrectomy may also help “flush” toxic metabolites out of the kidney through the unclamped renal vein better than the passive efflux that might occur in the setting of a completely occluded renal artery.

There are several limitations to our study. First, a relatively small number of animals were used and, as mentioned previously, the flow probe that was used to calibrate blood flow produced variability in the measurements, most likely due to unwieldy size of the probe. As a result, finer sub-categorizations of blood flow could not be determined and animals were grouped into only three groups: 0%, 10% and 25%. Secondly, our experience revealed that blood flow in a partially-clamped artery can vary when the kidney is being manipulated. While all efforts were made to keep the blood flow constant during the partial nephrectomy, variation did seem to occur

during this short portion of the clamping interval such that there might be some overlap between the groups in the study (figure 2). Such variation in the 10% flow group in combination with inevitable variation in the exact amount of renal parenchyma removed from the kidney likely explains why 10% flow did not show statistically significant improvement in renal functional recovery compared to 0% renal artery flow despite significantly better $\%HbO_2$ levels in the kidney during the ischemia period. This variation, though short in duration, likely mimics that which would be seen if this technique was put into clinical use. Though the partial nephrectomy component of the experiment was designed to further reduce renal functional reserve and magnify any advantage to minimal renal perfusion, future studies to tease out any differences between 0% and 10% renal artery flow likely should exclude this step. On the other hand, since HSI demonstrated significant differences in tissue oxygenation between all 3 groups, more sensitive measures of renal function and injury unavailable to us could have identified advantages to as little as 10% preserved renal artery flow. Finally, our work was performed in a porcine model, which, though commonly used to study kidney surgery in lieu of humans, has several important differences from humans. Porcine kidneys have a greater tolerance to warm ischemia and tend to have a lower propensity for bleeding. While the amount of bleeding during partial nephrectomy with 25% RA flow was not problematic in this porcine model, it is possible that permitting this degree of blood flow during human partial nephrectomy could cause unacceptable bleeding. Future investigations should aim to elucidate these differences.

Finally, the findings of this study suggest that HSI is a very sensitive tool to assess renal oxygenation in real-time and in a non-invasive fashion. Given the likely clinical difficulties of positioning a vascular flow probe, a needle PO_2 or microdialysate probe,[37] and an adjustable clamp on the renal artery, our experience suggests that hyperspectral imaging of $\%HbO_2$ can be used as a surrogate measure of blood flow whereby renal oxygenation is “titrated”. As such, HSI may be uniquely poised to serve as both a research and clinical instrument in nephron-sparing surgery, allowing us to study the effect of various techniques in preserving renal tissue oxygenation and then to “individualize surgery” for our patients by manipulating oxyhemoglobin

levels on a minute-by-minute basis. One could envision a procedure where the clamp is adjusted to alter the blood flow, depending on intra-operative assessment of bleeding and tissue oxygenation.

6.2.1.6 Conclusion

Incomplete renal artery occlusion during porcine partial nephrectomy results in favorable renal oxygenation profiles with as little as 10% blood flow and appears to be reno-protective when 25% of baseline renal artery flow is preserved. Hyperspectral imaging is a very sensitive, non-invasive tool for the real-time monitoring of renal oxygenation and thereby, blood flow, and may facilitate intra-operative decision making to protect kidney function. This work has recently been submitted for publication at the Journal of Urology.

6.3 Preliminary Data using Visible Laparoscopic Hyperspectral Imaging System

Based on the open partial nephrectomies, a new system has been developed for laparoscopic procedures. The new a laparoscopic system replaces the larger and bulkier HQ2 camera with a DVC camera that consists of the same Sony ICX CCD chip in a much smaller casing. The development of the laparoscopic system has been challenging due to the fact that the entire system needs to be handheld and easily manipulated unlike the previous system which was set on a tripod stand.

Initial Images of laparoscopic nephrectomies were taken using the DVC camera and the visible OL490 and the standard less flexible liquid light guide designed by Optronics Laboratory. Figure 6.12 shows the preliminary data collected using this system. Although this worked well, it required a combined effort of the surgeons, who were already sterilized and a technician, who was handling the unsterilized camera. The inflexible nature of the liquid light guide made it difficult for both people to maneuver the system. Hence, initial tests were carried out using the standard karl storz light guide used in the operating room (OR) and it was determined that this light guide could be used for hyperspectral imaging purposes.

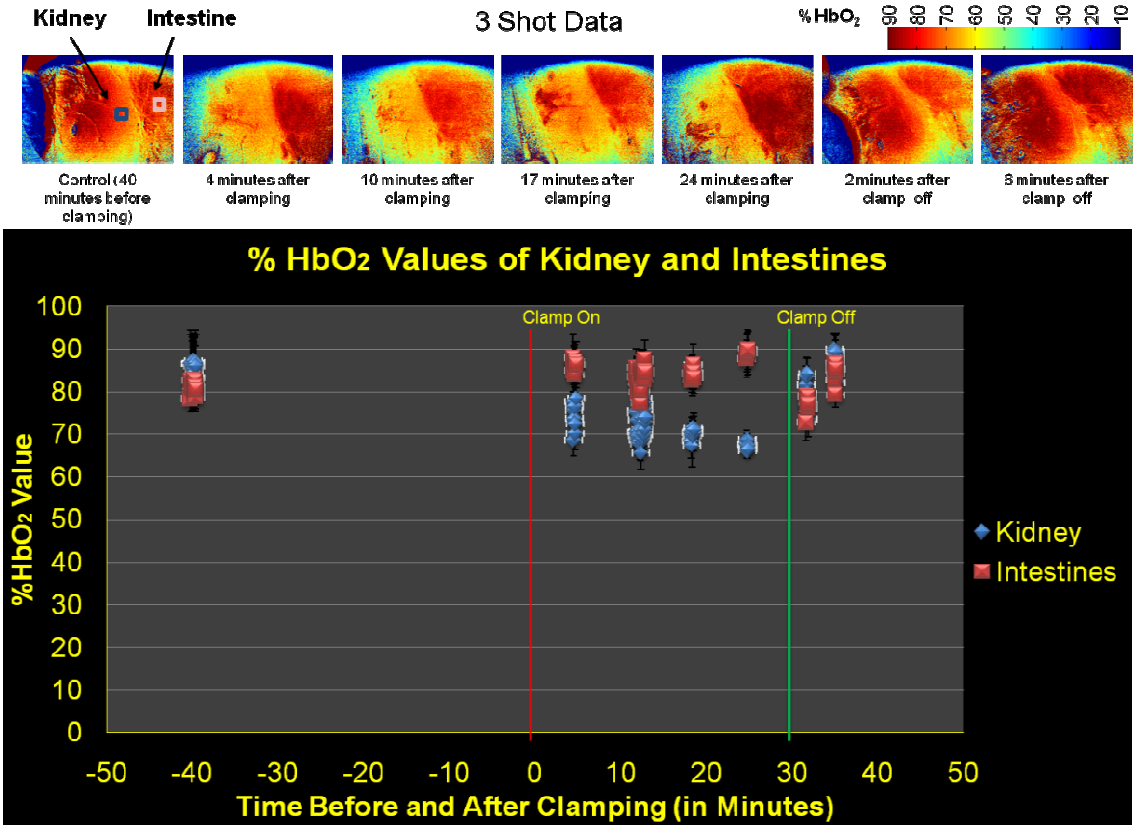

Figure 6.12 Hyperspectral imaging data of porcine laparoscopic surgery using the laparoscopic DLP® hyperspectral imaging system.

A standard 3-ccd coupler (c-mount) was used with the DVC camera to replace the initially machined mechanical coupler and a pentax lens. The laparoscopic probe could be swapped carefully but there was a risk of contaminating the sterilized surgical setting; so a method of bagging the camera was hence developed which allowed the surgeons to hold the camera while remaining sterile.

Moreover, in order to produce accurate results, the system needs to be at the same distance from the target tissue as the distance in which the background was taken. An ideal distance of 6 cm was determined during practical runs in porcine laparoscopic images. A temporary solution to setting the camera at this distance of 6cm has been to measure and attach a standard tom cat catheter. Although this method is not ideal, it is a temporary solution until a proper range finding technique is implemented.

Currently, the only remaining issue has been to take a background before the surgery without compromising the sterility of the system. The images in figure 6.13 show the recent preliminary data on the 126 shot method, from the system with the latter mentioned changes.

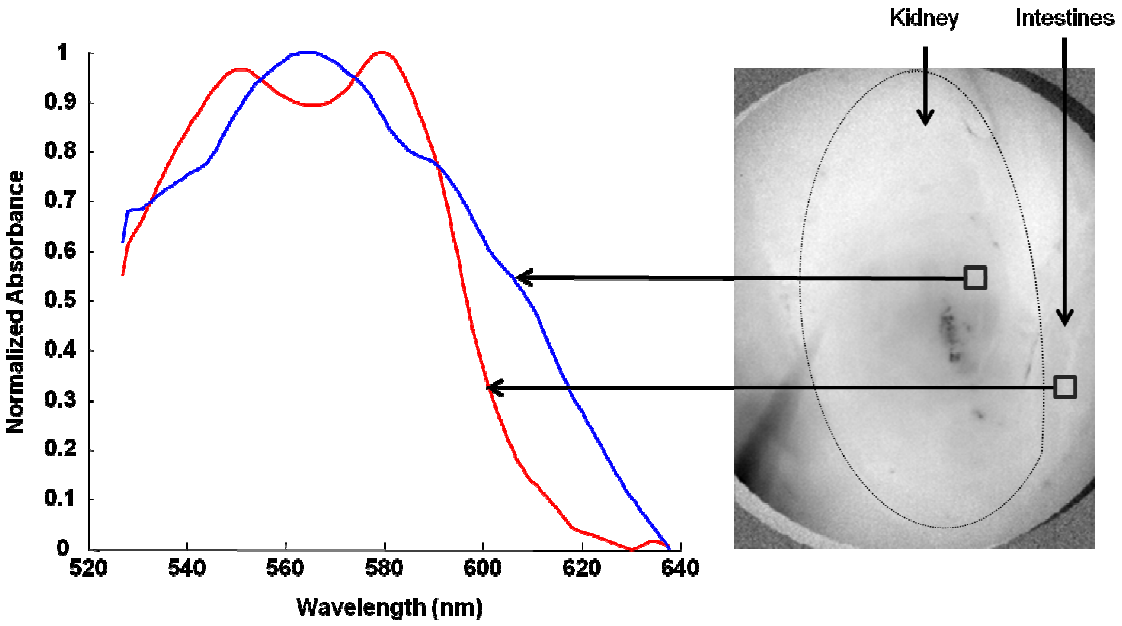

Figure 6.13 Normalized spectra (left) of oxyhemoglobin (red) and deoxyhemoglogin (blue) from sampled areas in the absorbance image (right) at 582nm.

6.4 Other Applications

6.4.1 Neurological Application: Stroke Detection and Aneurysm

Although hyperspectral Imaging has not yet been utilized to detect an aneurysm or monitor stroke during an open brain surgery in humans, preliminary data from the system, with experiments conducted on a rabbit brain suggests that the technology can be extremely useful in the neorological applications. The results from this initial imaging venture are as shown in figure 6.14. In this particular case, an area of the neural tissue was damaged while drilling to open up the skull. This area stayed deoxygenated during the entire imaging session while the other area, to which blood oxygenation was been cut off, turned deoxygenated over time. In order to access and clear aneurisms, brain surgeons clip specific feeding arteries of specific areas in the brain, so as to avoid blood loss during surgery. Blood flow to the area of interest is electro physiologically

monitored during these surgeries; but has not been effective in predicting post operative success of the surgery.

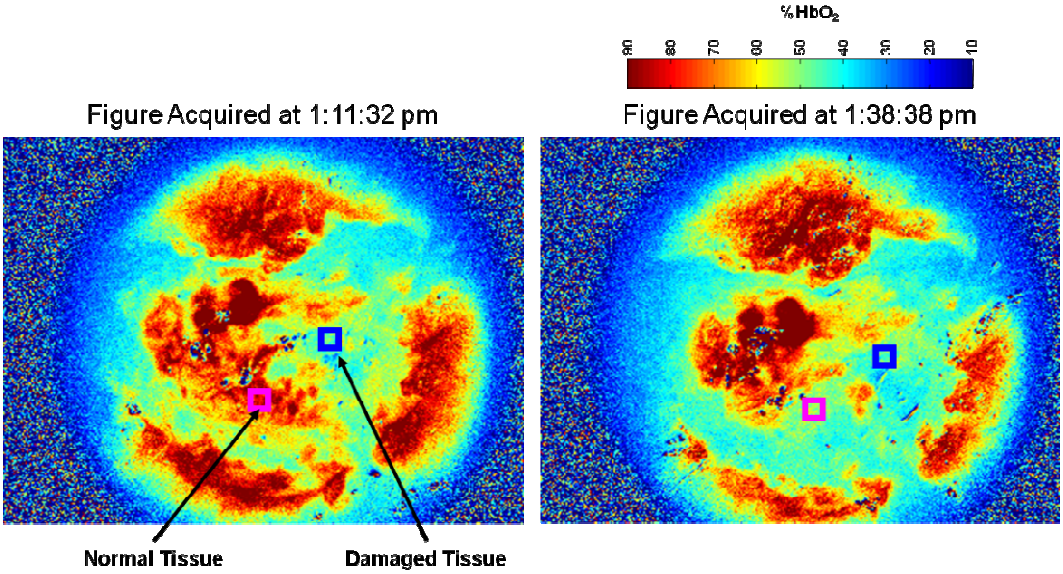

Figure 6.14 Hyperspectral images of normal and damaged areas in an exposed rabbit brain taken using visible hyperspectral imaging system before oxygen cutoff (a) and after oxygen cutoff (b).

Results from the rabbit model show that the system can be used to non-invasively monitor not just blood flow but actual tissue oxygenation in areas of brain in order to reduce the chances of a post operative stroke. Hence, hyperspectral imaging can be a novel approach in replacing current technologies and providing live, near video-rate, feedback of biochemical changes in neural tissue, inclusive but not limited to blood oxygenation.

6.4.2 Retinal Imaging for Diabetic Retinopathy and Age Related Macular Degeneration

Retinal imaging experiments were conducted on consenting humans, using the visible hyperspectral imaging system, to visualize vasculature in the retina of the eye. ELCAN Technologies, a part of Rathyeon, has actively been involved in further developing this method and has also explored areas in the near-infrared spectrum (NIR) for this purpose.

The preliminary tests shown in the figure 6.15 suggest that the visible system can be used in imaging vasculature of the eye. However, the limiting factor during this experiment was

that unlike other tissue, imaging the eye created challenges related to excessive movement. A specific alignment software has also been tested to correct for this movement artifact; but it has not proved to be very practical, due to its poor efficiency and accuracy for our method of analysis.

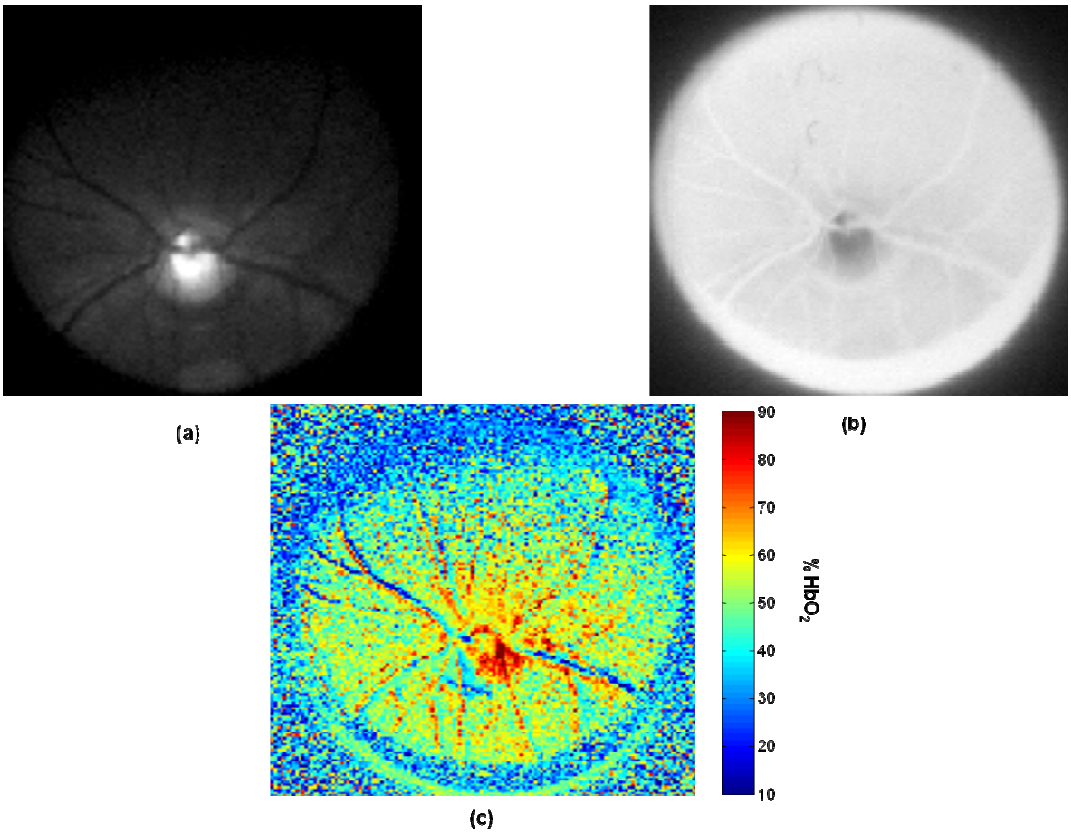

Figure 6.15 Hyperspectral imaging of human retina (a) An image of the vasculature in the human retina. (b) The absorbance image corresponding to a wavelength of 582nm and (c) A hyperspectral image showing oxyhemoglobin and deoxyhemoglobin levels in the vasculature. The blue areas indicate lower levels of oxyhemoglobin while the red areas indicate higher levels of oxyhemoglobin

ELCAN's focus on the project has improved the system to a point that spectral information can be collected while incorporating the movements using a fundus camera; and it has been found that collecting information on oxy- and deoxyhemoglobin are better when using the NIR spectral range.

6.4.3 Fluorescence Imaging Applications

Indo Cyanine Green (ICG) is a fluorescent material that emits light when excited with a certain wavelength of light. The chemical is FDA approved for intravenous injection in humans and has been used in many clinical and surgical settings to get anatomical information of different vasculatures in the human body. The capability of the DLP® system to illuminate the target with the specified spectral illumination method allows us to illuminate the ICG with the desired spectral bandpass more accurately. An NIR camera is then used to detect the NIR emission of the excited chemical. A test for this method was conducted by Michael Mangum, wherein, the vascular structures in a human placenta were injected by with ICG; and the emission was recorded as shown in figure 6.16.

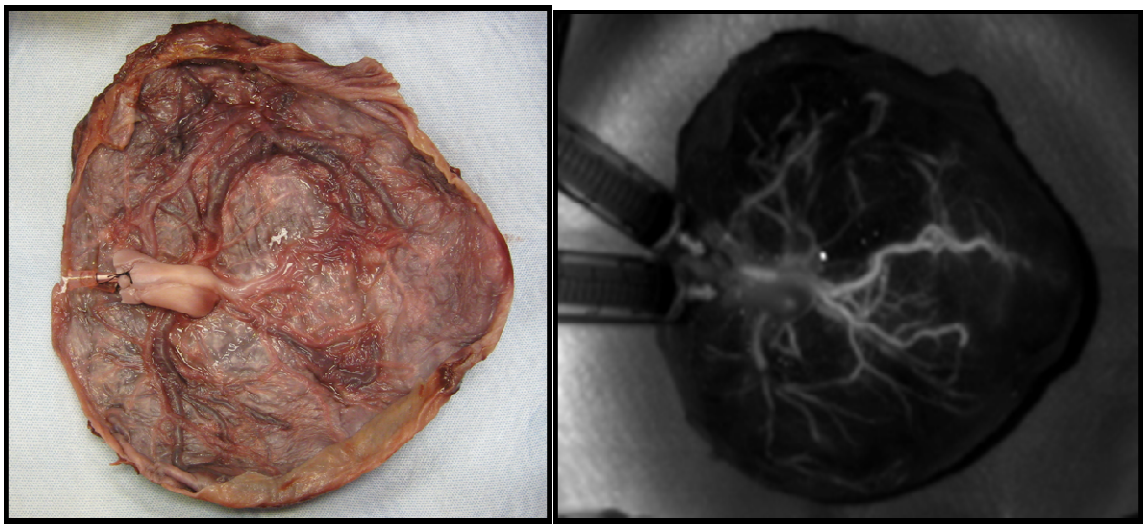

Figure 6.16: A human placenta (left) and an image of the placenta being injected with ICG (right). The flexible spectral illumination capability of the DLP® system allows more efficient fluorescence imaging.

6.4.4 Plastic Surgery

One of the recent exciting ventures of the visible system has been imaging skin flaps during plastic surgery in order to detect biochemical properties of the flaps, specifically oxy and deoxyhemoglobin. A project with Dr. Saint-Cyr at UTSW has shown that the visible system can help detect well perfused sections of the skin flaps for selection during breast reconstruction,

specifically for patients that have undergone a mastectomy. Figure 6.17 shows hyperspectral images collected by Michael Mangum during one of these procedures. An average of the $\%HbO_2$ value was significantly different larger in the left flap compared to the right, suggesting that the left flap was more suitable for selection during the breast reconstruction surgery.

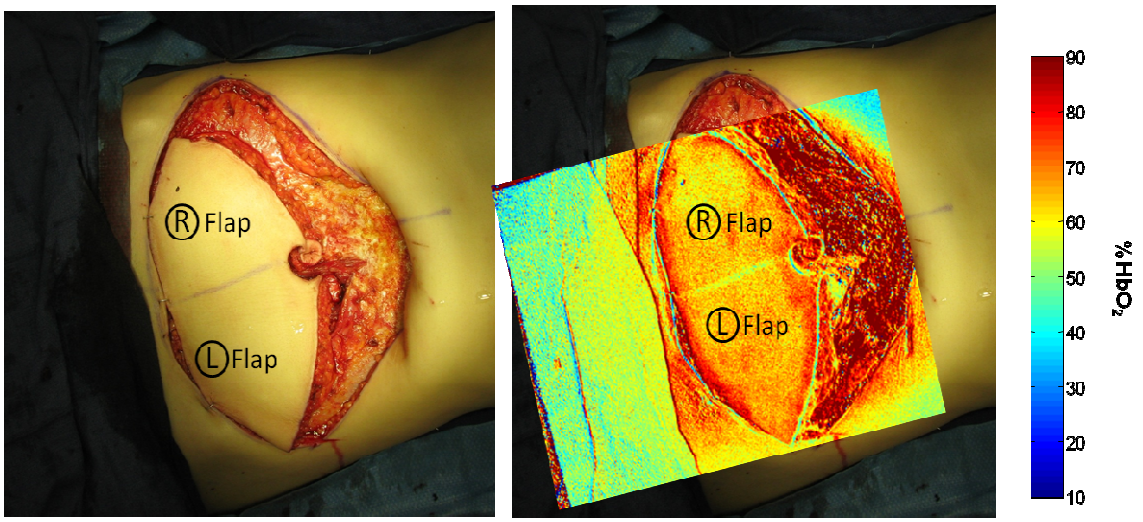

Figure 6.17: A regular Image of the flaps during plastic surgery (left) and hyperspectral image overlayed on the regular image (right) to show the tissue oxygenation map of the flaps.

6.4.5 NIR Imaging of Burns

Although the DLP® based NIR hyperspectral imaging system has not yet been fully developed for medical imaging purposes, a processing algorithm has developed for this system based on the water absorbance spectra. Previously however, an LCTF based hyperspectral Imaging system was developed and it has also been used for detecting levels of oxyhemoglobin in tissue. This NIR system was used to take the images shown in figure 6.18 of appendages for patients with severe burns. The same datacube was deconvoluted for both oxyhemoglobin and water. Although indistinguishable from the digital colored image in figure 6.18 (a), the areas with edema [figure 6.18 (c)] are not always the same areas with poor oxygenation [figure 6.18 (c)]. Having both the images from figure 6.18(b) and figure 6.18 (c) can help a surgeon decide whether to perform a fasciectomy, to release the water from the areas with apparent edema, or perform an amputation to save the remaining healthy tissue. These LCTF based results show that

the DLP® system can also be used for similar applications given the availability of correct reference spectra for the biochemical change of interest.

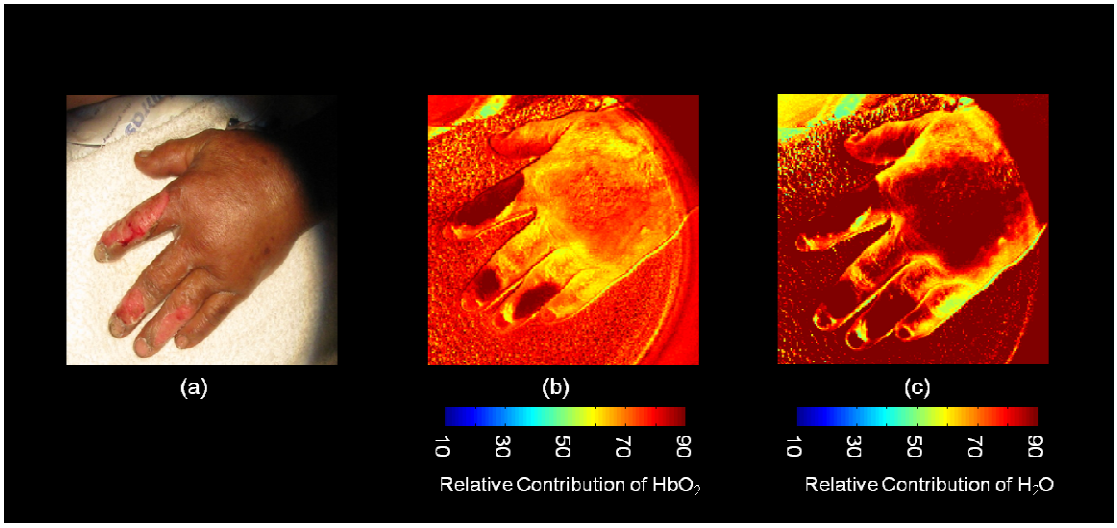

Figure 6.18 Images from an LCTF based NIR hyperspectral imaging system (a) A colored digital image of the hand of a patient with severe burns, (b) hyperspectral image of the hand data deconvoluted for relative contribution of oxyhemoglobin and (c) hyperspectral image of the hand data deconvoluted for water.

CHAPTER 7

CONCLUSION AND FUTURE DIRECTIONS

The study results from both porcine and human models suggests that the visible hyperspectral imaging system can be used in a surgical setting to successfully monitor changes in $\%HbO_2$ during partial nephrectomies. Clinical study conducted in these experiments, considering change in createnine levels as a factor to detect renal function, suggests that the visible hyperspectral imaging system can be very useful in predicting post operative renal function. Hence the research hypothesis is accepted.

7.1 DLP® Based Hyperspectral Imaging System

The DLP® based hyperspectral imaging system is a hardware and software integration of the illumination source, which works on the Digital Micromirror Device (DMD) technology developed by Texas Instruments; and a highly sensitive detector system which compromises of a CCD camera (visible system), a deep depleted CCD camera (mid-range system) or a VisGaAs or InGaAs camera (NIR system).

Currently four different DLP® based hyperspectral imaging systems have been developed in the laboratory of biomedical imaging at The University of Texas at Arlington. Amongst the four systems, two of the systems operate in the visible range covering a wavelength range of 380nm to 780nm, one of the systems operates in the VIS-NIR region covering a wavelength range from 525 nm to 1050 nm, and the fourth system operates in the NIR region covering a wavelength range from 760 nm to 1600 nm.

The DLP® based hyperspectral imaging system is a novel invention that can be used in various clinical and surgical applications in the medical field to provide real-time, near video rate information of biochemical changes in tissue. The visible hyperspectral imaging system has been

used to collect data on complete and partial nephrectomies in both porcines as well has humans. After the successful use of the DLP® based visible hyperspectral system in clinical and surgical settings, a new laparoscopic DLP® based visible hyperspectral system has been developed. The laparoscopic system comprises of the same DLP® based Ilumination source (OL490) as the system used for open partial nephrectomies but replaces the HQ2 camera by a much smaller and lighter DVC camera. The DVC camera consists of the same Sony ICX CCD and can be used to hardware trigger the DLP® system making the overall system much faster compared to the HQ2 system. The system is handheld and easily maneuverable. Preliminary experimental results from this system support its usability for future laparoscopic surgery applications.

7.2 Surgical and Clinical Studies of the DLP® Hyperspectral Imaging System

7.2.1 Renal Function Analysis using the DLP® *based Visible Hyperspectral System*

Human studies, using the DLP® based visible hyperspectral system, conducted on 21 patients suggested that a 20.0 percent decrease in $\%HbO_2$ from baseline after a median 9.5 minutes of hilar occlusion. The $\%HbO_2$ rebounded to levels between 80 and 90 percent of baseline after the initial drop to 80%. It plateaued at this level for the duration of the clamp time. The $\%HbO_2$ values returned to its baseline value within 5.8 minutes of clamp removal.

In another study conducted in the same human group, HSI showed that seven patients had a “low” average pre-clamp oxygenation (mean 69%) while the other 14 had a “high” HbO_2 (mean 79%). There was no difference in tumor size (p=0.22), hematocrit (p=0.93), clamp time (p=0.83), or pre-op eGFR (p=0.78) between the two groups. However, using creatinine values obtained post-operative day 1 or 2, it was determined that the median pre-operative change in eGFR in the high HbO_2 group was -3.5, while it was -14.8 in the low HbO_2 group (p=0.037).

In the porcine study, HSI showed that the nadir $\%HbO_2$ (i.e. the lowest recorded $\%HbO_2$) in the 0% renal arterial (RA) flow group was statistically lower than that seen in both the 25% and 10% RA flow groups (p=0.01 and 0.04, respectively). A serum creatinine test conducted on post-operative day 7 showed that renal function was found to favor 25% RA flow (p=0.048) compared to both 0% and 10% RA flow. This shows that incomplete renal artery occlusion during porcine

partial nephrectomy results in favorable renal oxygenation profiles with as little as 10% blood flow and appears to be reno-protective when 25% of baseline RA flow is preserved.

Hence, hyperspectral imaging system is a sensitive, non-invasive tool for the real-time monitoring of renal oxygenation, and thereby blood flow, which may facilitate in intra-operative decision-making to protect kidney function.

7.2.2 Other Applications of the DLP® *based Hyperspectral Systems*

Results from the DLP® based hyperspectral imaging systems in areas of neurology, ophthalmology, fluorescence imaging, plastic surgery and burns shows that the HIS systems can be used in various clinical and surgical applications in the medical field. Surgeons from all different fields have expressed interest in being able to utilize the system as a live guidance during surgical procedures.

Consumer level technology grows and changes very rapidly and quickly becomes obsolete in less than a few years. Surgeons have expressed concern in the lack of technological advancement in the current surgical settings. Healthcare industry has an immense effect in the economy of a country; so introducing new and improved technologies will not just benefits an individual but also benefit the entire nation. This new technology is focused on improving medical imaging technology and the presented results demonstrate that it can revolutionize healthcare methodologies, in surgical and clinical settings, known to date.

REFERENCES

1. Fong A, Bronson B, Wachman E. Advanced photonic tools for hyperspectral imaging in the life sciences. SPIE Newsroom 2008:2008.

2. Hornbeck LJ. Digital Light Processing™ for High-Brightness, High-Resolution Applications. 1997;141:1-16.

3. Hornbeck LJ. Digital Light Processing™: A New MEMS-Based Display Technology. 1996;117:1-23.

4. Texas Instruments. DLP Discovery 3000 Development Kits - DMD - DLP Technology. 2009;2009:1.

5. Saleh BEA, Teich MC. Fundamentals of photonics. Hoboken, NJ: John Wiley & Sons, Inc., 1991.

6. Francis, RP (2009), 'DLP Hyperspectral Imaging for Surgical and Clinical Utility', MS Thesis, University of Texas at Arlington, TX

7. Bowmaker JK, Dartnell HJA. Visual pigments of rods and cones in a human retina. Journal of Physiology 1980;298:501-511.

8. Sellar RG,3, Boreman GD2. Classification of imaging spectrometers for remote sensing applications. 2005;44:1-3.

9. Zuzak KJ, Naik SC, Alexandrakis G, Hawkins D, Behbehani K, Livingston EH. Characterization of a near-infrared laparoscopic hyperspectral imaging system for minimally invasive surgery. Anal Chem 2007;79:4709-4715.

10. Kommera S. Spectroscopic Characterization of Biliary Tract Tissues In-Vivo to Assist Laparoscopic Cholecystectomy. UTA Masters Thesis 2006.

11. Nitzan M,2, Taitelbaum H. The measurement of oxygen saturation in arterial and venous blood. 2008;11:9-15.

12. Zuzak KJ, Schaeberle MD, Lewis EN, Levin IW. Visible spectroscopic imaging studies of normal and ischemic dermal tissue. Proc SPIE Int Soc Opt Eng 2000;3918:17-26.

13. Zuzak KJ, Schaeberle MD, Levin IW, Neil LE, Freeman J, McNeil JD, Cancio LC. Visible and infrared hyperspectral visualization of normal and ischemic tissue. Annu Int Conf IEEE Eng Med Biol Proc 1999;2:1118.

14. Zuzak KJ, Schaeberle MD, Levin IW, Neil Lewis E. Visible reflectance hyperspectral imaging: Characterization of a noninvasive, in vivo system for determining tissue perfusion. Anal Chem 2002;74:2021-2028.

15. Shah BB, Cavanagh HD, Petroll WM, Kothare AD, Gundabhat P, Behbehani K, Zuzak KJ. In-vivo microvasculature visualization using hyperspectral imaging. Proc SPIE Int Soc Opt Eng 2006;6080:60800U.

16. MacKinnon N, Stange U, Lane P, MacAulay C, Quatrevalet M. Spectrally programmable light engine for in vitro or in vivo molecular imaging and spectroscopy. 2005;44:2033-2040.

17. Smith SW. Ch. 25: Special imaging techniques. The Scientist and Engineer's Guide to Digital Signal Processingwww.dspguide.com, 1997. p. 423-450.

18. Naik SC. Characterization of a Novel, *In Vivo*, Laparoscopic Hyperspectral Imaging System for Minimally Invasive Surgery. UTA Masters Thesis 2006.

19. Kothare AD. Visible Hyperspectral Imaging System With Improved Capabilities for Translational Medicince Projects. UTA Masters Thesis 2005.

20. Webster JG, editor. Medical instrumentation: Application and design. 3rd ed. Hoboken, NJ: John Wiley & Sons, Inc., 1998.

21. Guo B, Gunn SR1, Damper RI1,2, Nelson JDB2. Band selection for hyperspectral image classification using mutual information. 2006;3:522-526.

22. Du Z, Jeong MK1,3, Kong SG1,2. Band selection of hyperspectral images for automatic detection of poultry skin tumors. 2007;4:332-339.

23. Roberts DA1, Gardner M1, Church R1, Ustin S2, Scheer G2, Green RO1,3. Mapping chaparral in the Santa Monica Mountains using multiple endmember spectral mixture models. 1998;65:267-279.

24. Klabunde RE. Cardiovascular physiology concepts. : Lippincott Williams & Wilkins, 2004.

25. Gong EM, Zorn KC, Orvieto MA, Lucioni A, Msezane LP, Shalhav AL. Artery-only occlusion may provide superior renal preservation during laparoscopic partial nephrectomy. Urology 2008;72:843-846.

26. Quaresima V,3, Sacco S, Totaro R, Ferrari M. Noninvasive measurement of cerebral hemoglobin oxygen saturation using two near infrared spectroscopy approaches. 2000;5:201-205.

27. Frank RN. Diabetic Retinopathy. N Engl J Med 2004;350:48-58.

28. Novick AC. Renal hypothermia: in vivo and ex vivo. Urol Clin North Am. 1983; **10**: 637.

29. Zuzak KJ, Schaeberle MD, Gladwin MT et al. Noninvasive determination of spatially resolved and time-resolved tissue perfusion in humans during nitric oxide inhibition and inhalation by use of a visible-reflectance hyperspectral imaging technique. Circulation 2001; **104**: 2905.

30. Tracy CR, Terrell JD, Francis RP et al. Characterization of renal ischemia using DLP hyperspectral imaging: A pilot study comparing artery-only occlusion versus artery and vein occlusion. J Endourol 2010; **24**: 321.

31. Crane NJ, McHone B, Hawksworth J et al. Enhanced surgical imaging: Laparoscopic vessel identification and assessment of tissue oxygenation. J Am Coll Surg 2008; **206**:1159.

32. Crane NJ, Gillern SM, Tajkarimi K et al. Visual enhancement of laparoscopic partial nephrectomy with 3-charge coupled device camera: assessing intraoperative tissue perfusion and vascular anatomy by visible hemoglobin spectral response. J Urol 2010; **184**: 1279.

33. Zuzak KJ, Gladwin MT, Cannon RO III et al. Imaging hemoglobin oxygen saturation in sickle cell disease patients using noninvasive visible reflectance hyperspectral techniques: Effects of nitric oxide. Am J Physiol Heart Circ Physiol 2003; **285**:H1183.

34. Song C, Bang JK, Park HK et al. Factors influencing renal function reduction after partial nephrectomy. J Urol 2009; **181**:48.

35. Thompson RH, Lohse FI, Saad IR et al. The impact of ischemia time during open nephron sparing surgery on solitary kidneys: a multi-institutional study. J Urol 2007; **177(2)**:471.

36. Bensalah K, Raman JD, Zeltser IS et al.: A comparison of kidney oxygenation profiles between partial and complete renal artery clamping during nephron sparing surgery in a porcine model. Can J Urol 2009; 16: 4632-8.

37. Raman JD, Bensalah K, Bagrodia A et al.: Comparison of tissue oxygenation profiles using 3 different methods of vascular control during porcine partial nephrectomy. Urology 2009; 74: 926-31.

38. Zuzak K, Francis R, Wehner E et al.: Dlp hyperspectral imaging for surgical and clinical utility. . Proc SPIE 2009: 7170-5.

39. Orvieto MA, Zorn KC, Mendiola F et al.: Recovery of renal function after complete renal hilar versus artery alone clamping during open and laparoscopic surgery. J Urol 2007; 177: 2371-4.

40. Fergany AF, Hafez KS and Novick AC: Long-term results of nephron sparing surgery for localized renal cell carcinoma: 10-year followup. J Urol 2000; 163: 442-5.

41. Gill IS, Kavoussi LR, Lane BR et al.: Comparison of 1,800 laparoscopic and open partial nephrectomies for single renal tumors. J Urol 2007; 178: 41-6.

42. Collins GM, Green RD, Boyer D et al.: Protection of kidneys from warm ischemic injury. Dosage and timing of mannitol administration. Transplantation 1980; 29: 83-4.

43. Zuzak KJ, Naik SC, Alexandrakis G et al.: Intraoperative bile duct visualization using near-infrared hyperspectral video imaging. Am J Surg 2008; 195: 491-7.

44. Crane NJ, Pinto PA, Hale D et al.: Non-invasive monitoring of tissue oxygenation during laparoscopic donor nephrectomy. BMC Surg 2008; 8: 8.

45. Holzer MS, Best SL, Jackson N, Thapa A, Mir SA, Donnally CJ, Rao S, Wehner E, Raj GV, Livingston E, Cadeddu JA, and Zuzak KJ.: Renal oxygenation measurement during partial nephrectomy using DLP® hyperspectral imaging predicts post-operative renal function. World Congress of Endourology meeting, Chicago, IL, 2010.

BIOGRAPHICAL INFORMATION

Having graduated from St. Xavier's school in Nepal, Abhas pursued an Electrical and Electronics engineering degree from Kathmandu University, Nepal. He majored in telecommunication engineering during his undergraduate degree with involvements in multiple yearly electrical and electronic projects until the third year of his degree. A sudden discovery that his father had multiple infarctions in the left frontal lobe of his brain, following a seizure, instigated his interest in the biomedical engineering field. This created an opportunity for his final year biomedical project for recognizing and counting white blood cells (WBCs) in blood samples, using neural networks analysis and digital image processing. Working with a pathologist at the Himalayan hospital in Kathmandu helped him realize the lack of technical advancements in the field of health care, band showed him the tremendous opportunity of growth in this particular field. After his undergraduate degree, he applied to the biomedical engineering program at the University of Texas at Arlington (UTA), which is a joint program between UTA and The University of Texas Southwestern Medical Center (UTSW). He was approached by Dr. Karel Zuzak for a research assistantship position in the laboratory of biomedical imaging (LBI). During his research at LBI, he worked on the hyperspectral imaging (HSI) system for medical imaging. He worked extensively in data acquisition, statistical analysis and presentations. He also developed a new HSI system for laparoscopic applications. After initial work in the fields of neurology, ophthalmology and urology, his primary focus narrowed down to the urological applications of the HSI system. The projects he worked on were primarily funded by Texas Instruments (TI). He was actively involved in imaging partial nephrectomies in both porcines and humans, and through his work he has demonstrated the effectiveness of the HSI system for clinical and surgical applications. He hopes to continue research in this field and help translate this research grade system into industry grade equipment.